

Two Plus Four Equals Three—Iron(II)/Iron(IV) Comproportionation as an Additional Pathway for Iron(IV)-Oxido Reactions

Niko S. W. Lindlar né Jonasson, Annika Menke, Laura Senft, Andrea Squarcina, David Schmidl, Katherine Fisher, Serhiy Demeshko, Jan C. Kruse, Thomas Josephy, Peter Mayer, Jonathan Gutenthaler-Tietze, Peter Comba, Franc Meyer, Ivana Ivanović-Burmazović, and Lena J. Daumann*



Cite This: <https://doi.org/10.1021/acs.inorgchem.4c04518>



Read Online

ACCESS |



Metrics & More

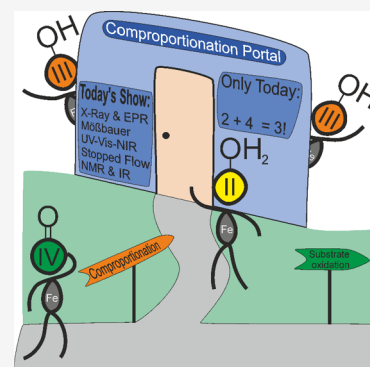


Article Recommendations



Supporting Information

ABSTRACT: Iron enzymes are ubiquitous in nature. In particular, enzymes with iron–oxygen cofactors as active sites perform a vast variety of reactions. Both iron(III)-hydroxido and iron(IV)-oxido species have been observed to play a catalytically active role. In order to complement biochemical investigations, a large variety of synthetic compounds using these motifs were synthesized in past decades to study and understand their inherent reactivity. One such synthetic model complex is $[\text{Fe}^{\text{IV}}(\text{O})(\text{Py}_5\text{Me}_2)]^{2+}$, ($\text{Py}_5\text{Me}_2 = 2,6\text{-bis}(1,1\text{-bis}(2\text{-pyridyl)ethyl)pyridine}$, henceforth labeled L1), which was used as a model complex for epigenetically relevant iron(II)/ α -ketoglutarate-dependent ten-11 translocation 5-methylcytosine dioxygenases (TET). Additionally, $[\text{Fe}^{\text{III}}(\text{OH})(\text{Py}_5(\text{OH})_2)]^{2+}$ ($\text{Py}_5(\text{OH})_2 = \text{pyridine-2,6-diylbis}[\text{di}(\text{pyridin-2-yl)methanol}$, henceforth labeled L2) was tested as a lipoyxygenase model. We have complemented the available complexes of these related pentapyridyl complexes to include all oxidation states II–IV and performed detailed spectroscopic and spectrometric investigations. We found that iron(II) and iron(IV)-oxido compounds (cross-)comproportionate readily to form iron(III)-hydroxido species, which represents a major side reaction for model complex investigations. We also investigated the oxidative reactivity of a new iron(IV)-oxido complex.



INTRODUCTION

Iron enzymes are ubiquitous in nature, and synthetic iron complexes have been used for decades to study these. In particular, iron(III)-hydroxido^{1–7} and iron(IV)-oxido^{8–14} complexes have been at the center of scientific interest. This is due to the involvement of these species in a multitude of enzymatic transformations. Two well-studied systems are lipoyxygenases,^{15–19} which contain an iron(III)-hydroxido active site, and taurine dioxygenases (TauD),^{20–23} which incorporate an iron(IV)-oxido center. Both enzymes are nonheme iron dioxygenases, while TauD specifically belongs to the iron(II)/ α -KG-dependent enzyme superfamily. Lipoyxygenases are typically thought to abstract a hydrogen atom from the fatty acid substrate via an iron(III)-hydroxido species, yielding a radical species. This is then thought to react with molecular oxygen, which is followed by cleavage of the substrate.^{17–19,24} The consensus mechanisms for TauD, on the other hand, involves the formation of an iron(IV)-oxido species, which abstracts a hydrogen atom from the substrate. This is followed by rebound hydroxylation to generate the product (Figure 1D).^{20–23,25,26} Subsequent reactions might lead to demethylation, ring closure, ring expansion, desaturation, and other transformations.²⁷

In synthetic (model) compounds, several pathways are observed after the initial H-atom abstraction step. A common feature in iron(III)-hydroxido chemistry is the prevalence of these compounds to form μ -O-bridged or μ -OH-dinuclear compounds.^{28–30} A recent, representative example is the bispidine-based system described by Abu-Odeh et al. in 2021.¹⁴ Using high-resolution electrospray ionization mass spectrometry (HR-ESI-MS), the authors observed an iron(IV)-oxido species upon oxidation of $[\text{Fe}^{\text{II}}(\text{bisp})\text{Cl}_2]$ (bisp = dimethyl 3,7-dimethyl-9-oxo-2,4-di(pyridin-2-yl)-3,7-diazabicyclo[3.3.1]nonane-1,5-dicarboxylate) with ⁵PhIO (⁵PhIO = 1-(*tert*-butylsulfonyl)-2-iodosylbenzene) in acetonitrile. In addition, $[(\text{bisp})\text{Fe}^{\text{III}}\text{—O—Fe}^{\text{III}}(\text{bisp})]^{2+}$ was also observed in MS measurements at low concentrations of the oxidant ⁵PhIO. The emergence of this species was attributed to the second-order reaction of the iron(IV)-oxido species with

Received: October 23, 2024

Revised: December 9, 2024

Accepted: January 10, 2025

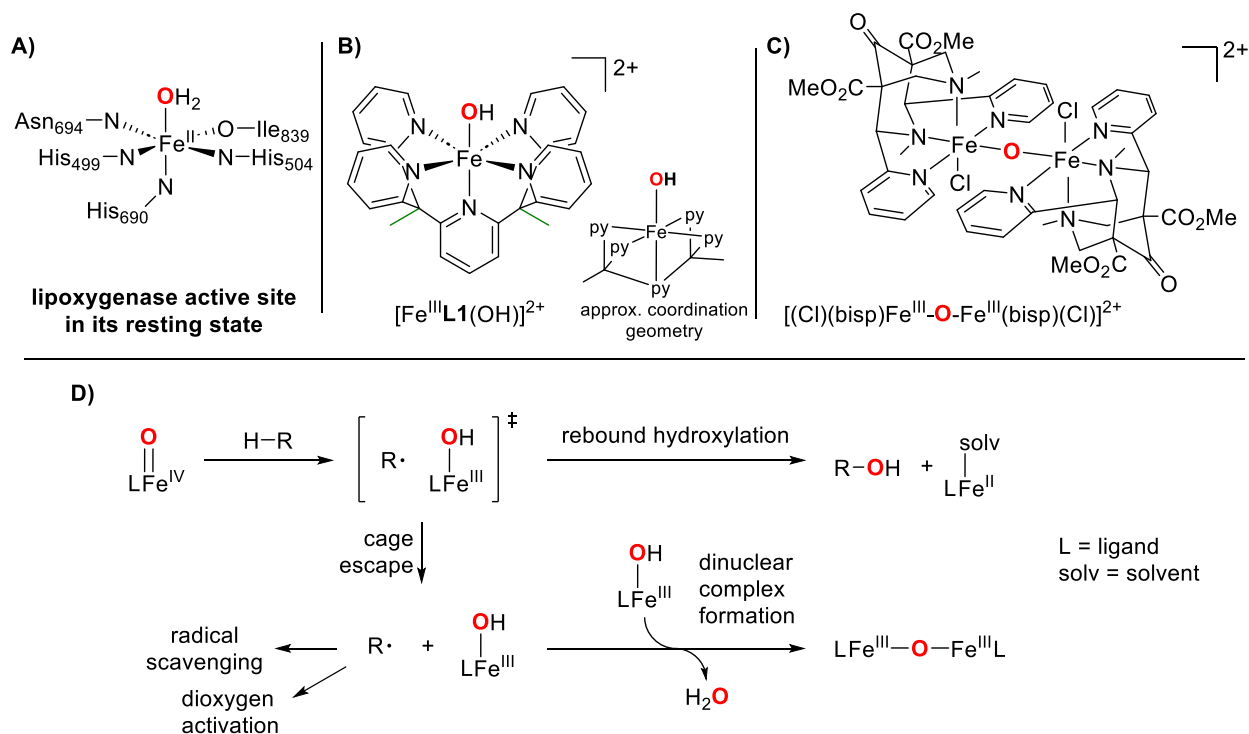
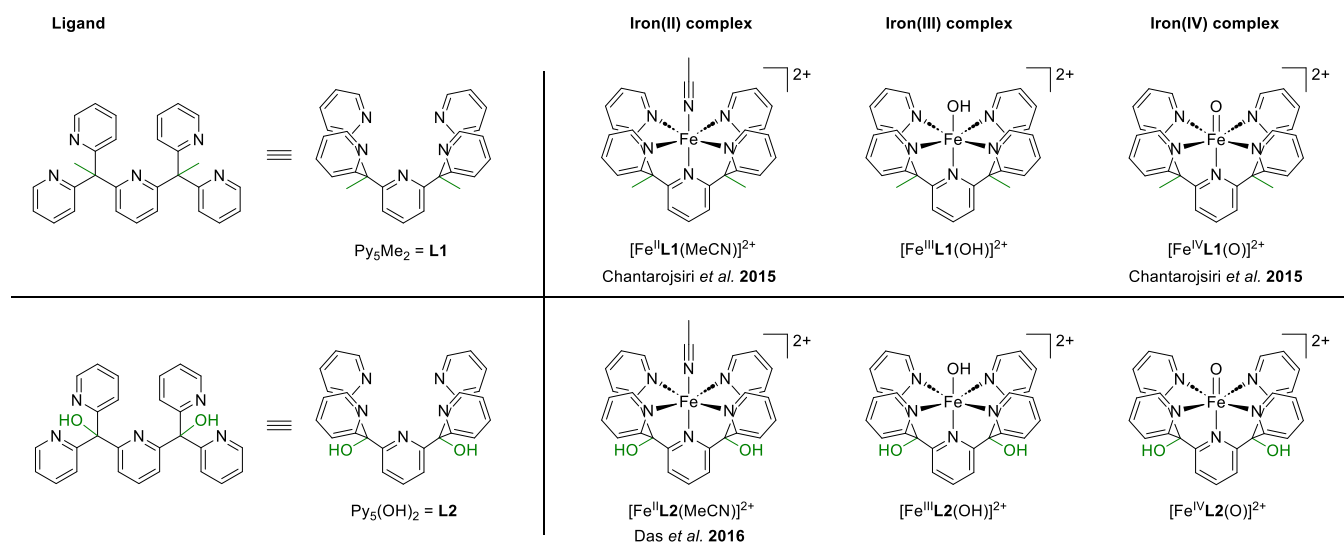


Figure 1. (A) Representation of the lipoygenase active site in its resting state according to Minor et al.³² (B) New iron(III)-hydroxido complex reported in this work. (C) Dinuclear iron(III)-oxido complex reported by Abu-Odeh et al.¹⁴ (D) Proposed mechanisms for the reaction of iron(IV)-oxido species with organic substrates bearing C–H bonds: after the initial hydrogen atom transfer reaction, rebound hydroxylation leads to an iron(II) species and the hydroxylated substrate. “Escape” of the radical from the “iron cage” giving an iron(III)-hydroxido species has also been observed. This can further lead to dinuclear complex formation with another equivalent of iron complex or scavenging of the radical or reaction with O_2 , depending on the conditions. Adapted from Cho et al.³³

Chart 1. Overview of the Ligands and Corresponding Iron(II), Iron(III), and Iron(IV)-Oxido Complexes Used in This Work⁴



⁴Counter ions: triflate (iron(II) and iron(III) species) and cerium nitrate (iron(IV)-oxido species). Spectroscopic and spectrometric data on newly synthesized compounds can be found in the [Supporting Information](#) and is referenced when applicable. It has to be noted here that the co-ligand of the iron(II) species is exchanged in solution by solvent molecules (see [Figure S14](#), p 18), and the nomenclature used in the paper refers to the actual species present in solution ($[\text{Fe}^{\text{II}}\text{L1}/\text{L2}(\text{OH}_2)]^{2+}$ in water) and not necessarily to the complex applied in the experiment.

62 unreacted iron(II) precursor. Other works have described
63 similar comproportionation (or disproportionation of iron-
64 (III)) behavior, e.g., the equilibrium between a tetracarbene-
65 coordinated μ -oxidodiiron(III) complex with its iron(IV)-
66 oxido and iron(II) derivatives.³¹

In addition to several dinuclear iron(III) complexes with
67 terminal hydroxido ligands,^{34–36} several mononuclear iron(III)
68 complexes have been described in the literature.^{2,5–7,37}
69 However, the isolation, especially of iron(III)-hydroxido
70 species, is often complicated, for example, by their tendency
71 to form μ -oxido-bridged diiron(III) species as discussed above. 72

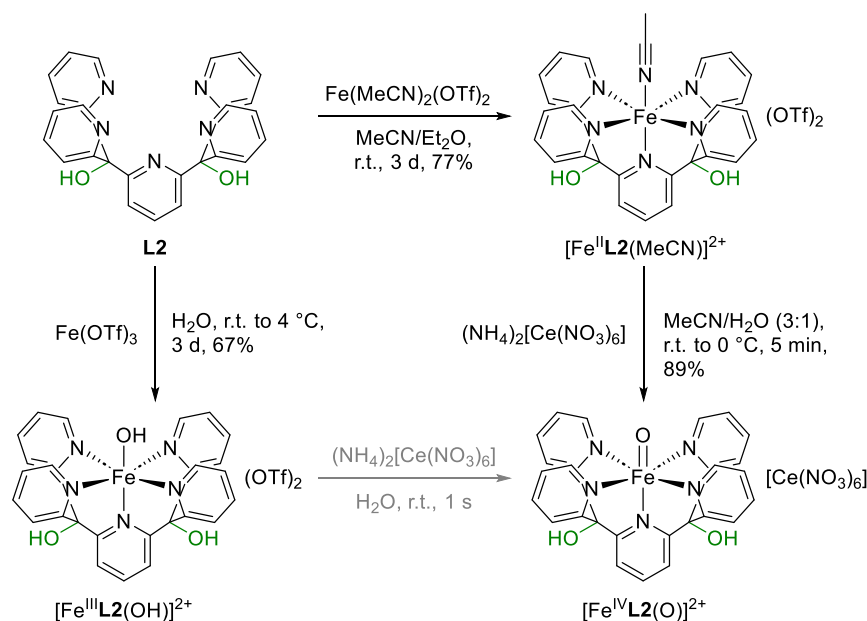


Figure 2. Synthesis of iron complexes $[\text{Fe}^{\text{II}}\text{L2}(\text{MeCN})]^{2+}$, $[\text{Fe}^{\text{III}}\text{L2}(\text{OH})]^{2+}$, and $[\text{Fe}^{\text{IV}}\text{L2}(\text{O})]^{2+}$ from ligand **L2** according to (modified) literature procedures.^{3,8,9}

73 The reported examples of mononuclear iron(III)-hydroxido
74 complexes often consist of ligand systems similar to those
75 employed in this work. In the present work, we report the
76 synthesis and isolation of two new mononuclear, low-spin
77 iron(III)-hydroxido complexes and present their X-ray
78 structures as well as EPR, Mössbauer, and UV–vis–NIR
79 spectra.

80 In our previous work, we studied the iron(IV)-oxido
81 complex $[\text{Fe}^{\text{IV}}\text{L1}(\text{O})]^{2+}$ as a functional model for the
82 epigenetically relevant iron(II)/ α -ketoglutarate-dependent en-
83 zyme TET (ten-11 translocation 5-methyl-cytosine dioxyge-
84 nase).^{9–11} This complex was first described by Chantarojsiri et
85 al. in 2015.⁸ It is capable of hydroxylating organic compounds
86 such as ethylbenzene sulfonic acid (EBS) and the biologically
87 more relevant 5-methyl cytosine (5mC)/5-methyl cytidine
88 (5mdC) as well as oligonucleotides containing 5mC.¹⁰ In the
89 present work, we report the synthesis and isolation of a new
90 iron(IV)-oxido complex including the corresponding Mössbauer
91 and UV–vis–NIR spectra as well as a preliminary
92 reactivity study.

93 ■ RESULTS AND DISCUSSION

94 In this work, the repertoire of known iron complexes
95 containing pentapyridyl ligands of the Py5-type was expanded.
96 Two complete series of iron(II), iron(III), and iron(IV)
97 species of the Py_5Me_2 and $\text{Py}_5(\text{OH})_2$ ligand systems are
98 presented here, including two new mononuclear iron(III)-
99 hydroxido and a new iron(IV)-oxido species. All synthesized
100 compounds were characterized using electron paramagnetic
101 resonance (EPR), Mössbauer, and UV–vis–NIR spectroscopy
102 as well as cyclic voltammetry and ultrahigh-resolution low-
103 temperature mass spectrometry (cryo-UHR–MS). In addition,
104 a comparative reactivity study containing several substrates
105 with C–H bonds was performed. **Chart 1** shows the ligands
106 and iron complexes as well as the nomenclature applied in this
107 work.

108 **Characterization of New Iron Complexes and**
109 **Comparison of the Two Ligand Systems.** When analyzing

reaction mixtures of $[\text{Fe}^{\text{IV}}\text{L1}(\text{O})]^{2+}$ with an epigenetically
110 relevant substrate (5-methyl cytosine, 5mC or 5-methyl-
111 deoxycytidine, 5mdC) in previous studies,^{9,10} we found
112 significant amounts of the iron(III) species $[\text{Fe}^{\text{III}}\text{L1}(\text{OH})]^{2+}$.
113 This was attributed to a side reaction consisting of an iron(II)/
114 iron(IV) comproportionation reaction (vide infra for detailed
115 discussion) that prompted us to synthesize and characterize
116 this mononuclear iron(III)-hydroxido complex.
117

The series of iron complexes for both ligand systems **L1** and
118 **L2** (**Chart 1**) was synthesized, and various spectroscopic and
119 spectrometric techniques as well as cyclic voltammetry were
120 applied for a thorough characterization of the new iron
121 complexes and for comparison studies among the different iron
122 species. Here, a short overview of the syntheses is presented;
123 synthetic details can be found at the end of this article.
124

Synthesis. Py_5Me_2 (**L1**) was synthesized according to a
125 modified literature procedure,⁸ as previously described in our
126 report on iron(IV)-oxido complex $[\text{Fe}^{\text{IV}}\text{L1}(\text{O})]^{2+}$ as a
127 functional model for TET enzymes.⁹ Complexes
128 $[\text{Fe}^{\text{II}}\text{L1}(\text{MeCN})]^{2+}$ and $[\text{Fe}^{\text{IV}}\text{L1}(\text{O})]^{2+}$ were then synthesized
129 according to literature procedures.⁸ Complex $[\text{Fe}^{\text{III}}\text{L1}(\text{OH})]^{2+}$
130 was prepared by suspending a finely ground powder of **L1** in
131 pure water and adding iron(III) triflate ($\text{Fe}(\text{OTf})_3$). The
132 solution immediately turned a deep, dark red. Crystals of the
133 iron(III)-hydroxido compound formed in a filtered aqueous
134 solution at 4 °C after 1 day. A similar iron(III)-hydroxido²
135 as well as an iron(III)-methoxido¹ species has been described
136 before by Goldsmith et al. with a ligand system bearing
137 methoxy instead of methyl/hydroxy groups (2,6-bis(bis(2-
138 pyridyl)methoxymethane)pyridine). The authors obtained this
139 complex by reacting the corresponding iron(II) species with
140 iodosylbenzene.
141

Ligand $\text{Py}_5(\text{OH})_2$ (**L2**) was synthesized according to a
142 modified literature procedure (**Figure 2**).² $[\text{Fe}^{\text{II}}\text{L2}(\text{MeCN})]-$
143 $(\text{OTf})_2$ was then synthesized using the same procedures as for
144 the corresponding iron(II) complex of **L1** ($[\text{Fe}^{\text{II}}\text{L1}(\text{MeCN})]-$
145 $(\text{OTf})_2$) that had previously been published by Chantarojsiri et
146 al.⁸ In 2016, Das et al. published their results on water
147

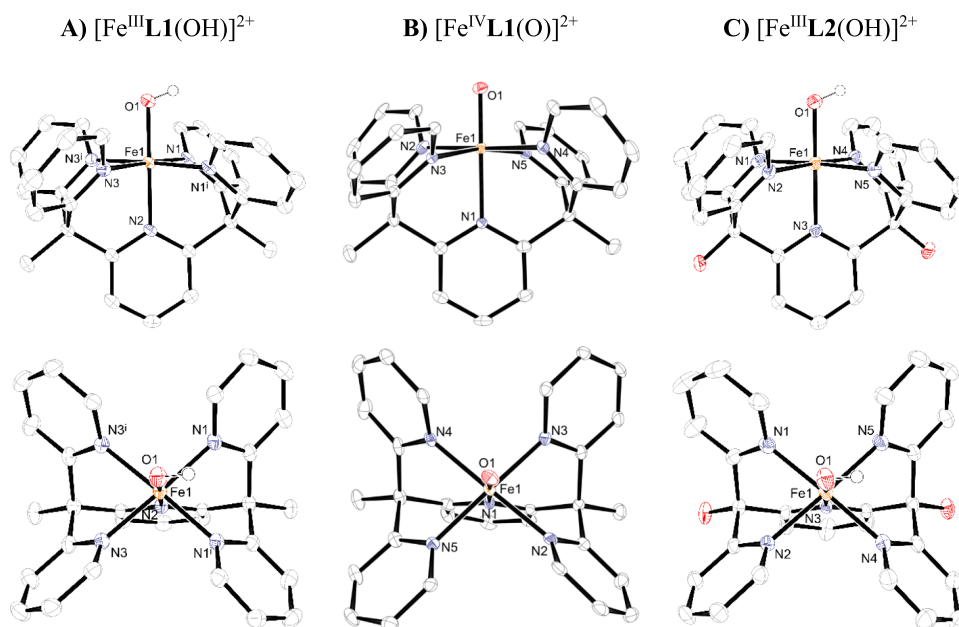


Figure 3. (A) Graphical representation of the crystal structures of $[\text{Fe}^{\text{III}}\text{L1}(\text{OH})]^{2+}$. Ellipsoids are drawn at 50% probability; hydrogen atoms, the counterion (^-OTf), and one cocrystallized water molecule were omitted for clarity. A full structure can be found in the [Supporting Information](#), p 50. (B) Graphical representation of the crystal structure of $[\text{Fe}^{\text{IV}}\text{L1}(\text{O})]^{2+}$, taken from Rasheed et al.¹³ Ellipsoids are drawn at 50% probability, and hydrogen atoms and the counterion ($[\text{Ce}(\text{NO}_3)_6]^{2-}$) were omitted for clarity. (C) Graphical representation of the crystal structure used for X-ray crystallography of $[\text{Fe}^{\text{III}}\text{L2}(\text{OH})]^{2+}$. Ellipsoids are drawn at 50% probability; hydrogen atoms, counterions (^-OTf), and two cocrystallized water molecules were omitted for clarity. A full structure can be found in the [Supporting Information](#), p 54.

148 oxidation using an iron-L2 system.³ Upon addition of
 149 ceric(IV) ammonium nitrate to $[\text{Fe}^{\text{II}}\text{L2}(\text{MeCN})](\text{BF}_4)_2$, the
 150 authors observed a band at $\lambda = 730$ nm in UV-vis-NIR
 151 spectroscopy, which they attributed to the formation of an
 152 iron(IV)-oxido species. The authors, however, could not
 153 isolate this compound. Applying the conditions published by
 154 Chantarojsiri et al.,⁸ i.e., oxidation of $[\text{Fe}^{\text{II}}\text{L2}(\text{MeCN})](\text{OTf})_2$
 155 in an acetonitrile/water mixture using 5.3 equiv of ceric(IV)
 156 ammonium nitrate, we were able to isolate $[\text{Fe}^{\text{IV}}\text{L2}(\text{O})][\text{Ce}-$
 157 $(\text{NO}_3)_6]$ as a green powder. Synthesis of $[\text{Fe}^{\text{III}}\text{L2}(\text{OH})]^{2+}$ was
 158 performed in the same way as that for $[\text{Fe}^{\text{III}}\text{L1}(\text{OH})]^{2+}$ (vide
 159 *supra*).

160 **Characterization by X-ray Crystallography.** The cations
 161 $[\text{Fe}^{\text{II}}\text{L1}(\text{MeCN})]^{2+}$ and $[\text{Fe}^{\text{IV}}\text{L1}(\text{O})]^{2+}$ are known in the
 162 literature and corroborated by our own measurements (not
 163 shown; refer to the [Supporting Information](#), p 48ff for
 164 crystallographic details including a table containing relevant
 165 bond lengths and angles and a comparison with published
 166 data). A structural study of $[\text{Fe}^{\text{IV}}\text{L1}(\text{O})]^{2+}$ using X-ray
 167 crystallography ([Figure 3B](#)) and ^1H NMR spectroscopy was
 168 published in 2019 by Rasheed et al.¹³ In this work, single
 169 crystals of $[\text{Fe}^{\text{IV}}\text{L1}(\text{O})]^{2+}$ suitable for X-ray crystallography
 170 were also obtained from an aqueous solution of
 171 $[\text{Fe}^{\text{IV}}\text{L1}(\text{O})]^{2+}/\text{CeCl}_3$ (1:3). Crystals of the iron(III)-hydroxido
 172 compound $[\text{Fe}^{\text{III}}\text{L1}(\text{OH})]^{2+}$ formed both after evaporation
 173 of water from a reaction mixture of $[\text{Fe}^{\text{IV}}\text{L1}(\text{O})]^{2+}$ with 5-
 174 methyl cytosine (used in this work, [Figure 3A](#)) and in a filtered
 175 aqueous solution of ligand L1 and iron(III)triflate at 4 °C after
 176 1 day (the obtained structure is identical, not shown).

177 A crystal structure of $[\text{Fe}^{\text{II}}\text{L2}(\text{MeCN})]^{2+}$ was reported in the
 178 literature³; however, no details were provided due to the poor
 179 quality of the crystals. We were able to obtain crystals of
 180 $[\text{Fe}^{\text{II}}\text{L2}(\text{MeCN})]^{2+}$ in good quality by diffusing diethyl ether
 181 into an acetonitrile solution of $[\text{Fe}^{\text{II}}\text{L2}(\text{MeCN})]^{2+}$ at room

temperature. A comparison with $[\text{Fe}^{\text{II}}\text{L1}(\text{MeCN})]^{2+}$ showed
 182 that almost identical parameters were obtained for both
 183 complexes (refer to the [Supporting Information](#), p 48 for
 184 relevant bond length and angle values and p 52 for a full
 185 structure of $[\text{Fe}^{\text{II}}\text{L2}(\text{MeCN})]^{2+}$.
 186

Crystals of $[\text{Fe}^{\text{III}}\text{L2}(\text{OH})]^{2+}$ were obtained in an aqueous
 187 solution at 4 °C ([Figure 3C](#)). Comparing the bond lengths in
 188 $[\text{Fe}^{\text{III}}\text{L1}(\text{OH})]^{2+}$ and $[\text{Fe}^{\text{III}}\text{L2}(\text{OH})]^{2+}$, the iron–oxygen bond
 189 in $[\text{Fe}^{\text{III}}\text{L2}(\text{OH})]^{2+}$ was found to be slightly longer than in
 190 $[\text{Fe}^{\text{III}}\text{L1}(\text{OH})]^{2+}$ (1.81 vs 1.79 Å, respectively), as were the
 191 iron–nitrogen bonds (averaged: 2.01 vs 2.00 Å, respectively).
 192 Apart from these minor discrepancies, the structures exhibit a
 193 high degree of similarity (refer to the [Supporting Information](#),
 194 p 48 for relevant bond length and angle values).
 195

A comparison of the crystallographic data obtained for
 196 $[\text{Fe}^{\text{III}}\text{L1}(\text{OH})]^{2+}$ with the literature-known data^{5,8,13} for
 197 $[\text{Fe}^{\text{II}}\text{L1}(\text{OH}_2)](\text{BF}_4)_2$ and $[\text{Fe}^{\text{IV}}\text{L1}(\text{O})]^{2+}$ (compare [Figure](#)
 198 [4A,B](#)) shows a shorter iron–oxygen bond length with
 199 Fe^{IV} increasing oxidation state. Similarly, the iron atom “moves”
 200 out of the coordinative plane of the four equatorial pyridine
 201 donors, which also lengthens the iron–nitrogen bond of the
 202 axial pyridine moiety ([Figure 4B](#)).
 203

In the literature, similar bond lengths were observed for
 204 chemically similar nonheme iron(IV) complexes, e.g.,
 205 $[\text{Fe}^{\text{IV}}(\text{O})(\text{SMe}_2\text{N}_4\text{Py})](\text{ClO}_4)_2$ (1.654 Å)¹³ or $[\text{Fe}^{\text{IV}}(\text{O})(\text{Bn}-$
 206 $\text{tpen})]^{2+}$ (1.616 Å)³⁸ and also in the nonheme iron enzyme
 207 taurine dioxygenase TauD (1.646 Å).³⁹ For the iron–nitrogen
 208 bond trans to the iron–oxygen bond, also similar values have
 209 been reported for related complexes such as $[\text{Fe}^{\text{IV}}(\text{O})-$
 210 $(\text{SMe}_2\text{N}_4\text{Py})](\text{ClO}_4)_2$ (2.042 Å)¹³ and $[\text{Fe}^{\text{IV}}(\text{O})(\text{Bn}-$
 211 $\text{tpen})]^{2+}$ (2.112 Å).³⁸ The observed iron–oxygen bond lengths
 212 in the two newly synthesized iron(III)-hydroxido complexes
 213 (~ 1.80 Å) are similar to or shorter than what has been
 214 reported for other iron(III)-hydroxido complexes (1.880 Å,⁴⁰ 215

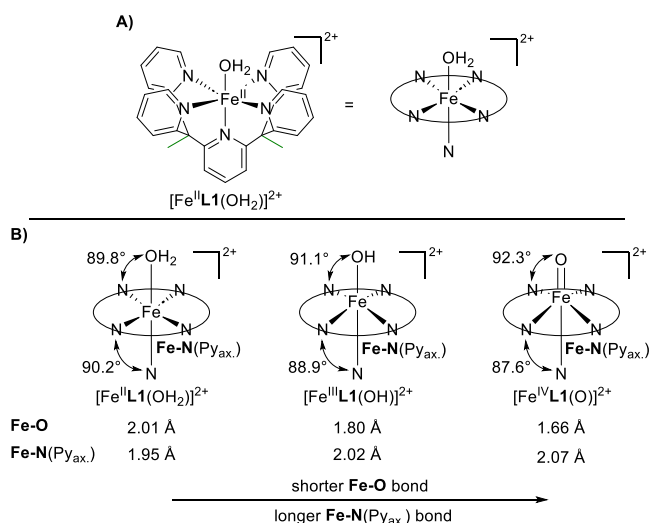


Figure 4. (A) Simplified graphical representation of the coordination environment of the iron(II) central ion in $[\text{Fe}^{\text{II}}\text{L1}(\text{OH}_2)](\text{BF}_4)_2$. (B) Graphical representation of the changes in coordination geometry between $[\text{Fe}^{\text{II}}\text{L1}(\text{OH}_2)]^{2+}$, $[\text{Fe}^{\text{III}}\text{L1}(\text{OH})]^{2+}$, and $[\text{Fe}^{\text{IV}}\text{L1}(\text{O})]^{2+}$ including selected bond lengths. Data for $[\text{Fe}^{\text{II}}\text{L1}(\text{OH}_2)](\text{BF}_4)_2$ and $[\text{Fe}^{\text{IV}}\text{L1}(\text{O})]^{2+}$ were taken from the literature.⁸ Additional angles and bond lengths are provided in the Supporting Information, p 48.

216 1.876 Å,⁴¹ or 1.872 Å⁴²). This is expected, as in the complexes
217 discussed herein, no hydrogen bonding interactions take place
218 that might elongate the iron–oxygen bond.

Characterization by Mössbauer Spectroscopy. The 219
Mössbauer spectra (Figure 5) of the newly synthesized 220
complexes $[\text{Fe}^{\text{III}}\text{L1}(\text{OH})]^{2+}$, $[\text{Fe}^{\text{III}}\text{L2}(\text{MeCN})]^{2+}$, 221
 $[\text{Fe}^{\text{III}}\text{L2}(\text{OH})]^{2+}$, and $[\text{Fe}^{\text{IV}}\text{L2}(\text{O})]^{2+}$ correspond well to the 222
assigned oxidation and spin states. All complexes of L1 are low- 223
spin (iron(II): $S = 0$; iron(III): $S = 1/2$; and iron(IV): $S = 1$), 224
as expected for the iron(II) and iron(IV) states from the 225
literature.⁸ For all three complexes of L2, both isomer shift and 226
quadrupole splitting parameters are nearly identical to those of 227
the complexes of L1, showing only a small influence of the 228
ligand periphery on the electronic structure around the iron 229
atom. Detailed information as well as Mössbauer spectra of the 230
literature-known species $[\text{Fe}^{\text{II}}\text{L1}(\text{MeCN})]^{2+}$ and 231
 $[\text{Fe}^{\text{IV}}\text{L1}(\text{O})]^{2+}$ are provided in the Supporting Information, p 232
47. The isomer shift and quadrupole splitting values we 233
observed for the iron(IV)-oxido complex $[\text{Fe}^{\text{IV}}\text{L2}(\text{O})]^{2+}$ are in 234
the same range of what is commonly observed in the literature 235
for similar complexes, e.g., $[\text{Fe}^{\text{IV}}(\text{O})(\text{N4Py}^{2\text{PhF}2})]^{2+}$ ($\delta = 0.03$ 236
 mm s^{-1} , $\Delta E_{\text{Q}} = 0.54 \text{ mm s}^{-1}$),⁴³ $[\text{Fe}^{\text{IV}}(\text{O})(\text{TMG}_3\text{tren})]^{2+}$ ($\delta = 0.09$ 237
 mm s^{-1} , $\Delta E_{\text{Q}} = -0.29 \text{ mm s}^{-1}$),⁴⁴ or $\text{Fe}^{\text{IV}}(\text{O})$ - 238
 $(\text{TMG}_2\text{dien})(\text{MeCN})]^{2+}$ ($\delta = 0.08 \text{ mm s}^{-1}$, $\Delta E_{\text{Q}} = 0.58 \text{ mm}$ 239
 s^{-1}).⁴⁵ Especially, the low isomer shift is typical for an 240
iron(IV)-oxo complex. The observed isomer shifts for the 241
newly synthesized iron(III)-hydroxido complexes are also in 242
agreement with values found in the literature, e.g., 243
 $[\text{Fe}^{\text{III}}\text{H}_3\text{buea}(\text{OH})]^{-}$ ($\delta = 0.32 \text{ mm s}^{-1}$), whereas the observed 244
quadrupole splitting differs from what is reported for this 245
complex ($\Delta E_{\text{Q}} = -0.82 \text{ mm s}^{-1}$), which is unsurprising, 246
considering the different ligand geometries. 247

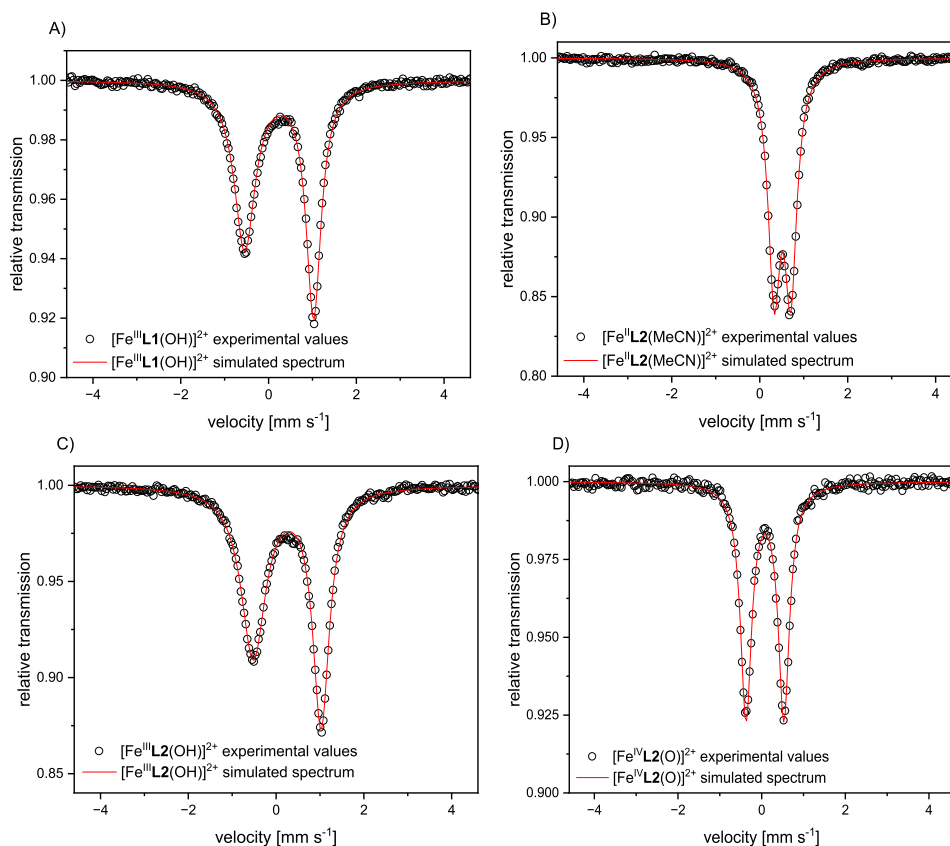


Figure 5. Experimentally obtained solid-state and simulated Mössbauer spectra and values of (A) $[\text{Fe}^{\text{III}}\text{L1}(\text{OH})](\text{OTf})_2$ ($\delta = 0.24 \text{ mm s}^{-1}$, $\Delta E_{\text{Q}} = 1.57 \text{ mm s}^{-1}$), (B) $[\text{Fe}^{\text{III}}\text{L2}(\text{MeCN})](\text{OTf})_2$ ($\delta = 0.52 \text{ mm s}^{-1}$, $\Delta E_{\text{Q}} = 0.38 \text{ mm s}^{-1}$), (C) $[\text{Fe}^{\text{III}}\text{L2}(\text{OH})](\text{OTf})_2$ ($\delta = 0.25 \text{ mm s}^{-1}$, $\Delta E_{\text{Q}} = 1.54 \text{ mm s}^{-1}$), and (D) $[\text{Fe}^{\text{IV}}\text{L2}(\text{O})][\text{Ce}(\text{NO}_3)_6]$ ($\delta = 0.08 \text{ mm s}^{-1}$, $\Delta E_{\text{Q}} = 0.35 \text{ mm s}^{-1}$). Mössbauer spectra were measured at 80 K.

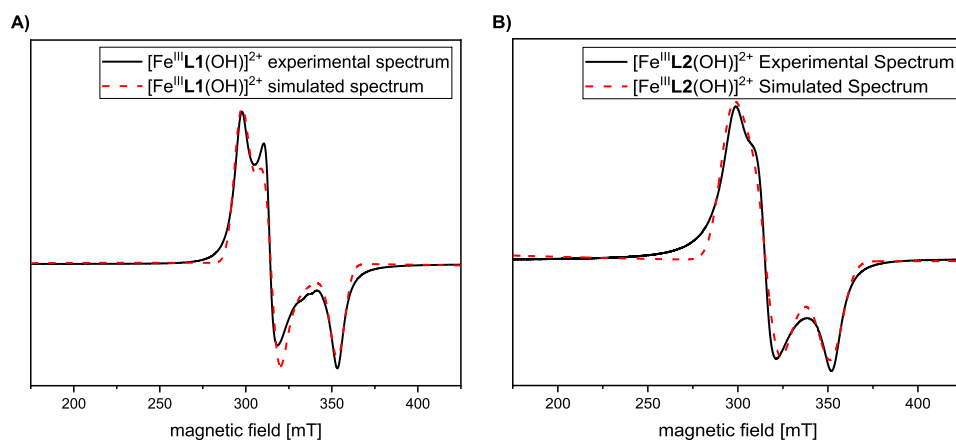


Figure 6. Experimentally obtained solid-state and simulated EPR spectra of (A) $[\text{Fe}^{\text{III}}\text{L1}(\text{OH})]^{2+}$ ($g = 2.32, 2.19, \text{ and } 1.95$) and (B) $[\text{Fe}^{\text{III}}\text{L2}(\text{OH})]^{2+}$ ($g = 2.33, 2.18, 1.96$). EPR spectra were measured at 298 K in X-band at 9.649818 and 9.649704 GHz, respectively; for more experimental details please refer to the [Supporting Information](#), p 4.

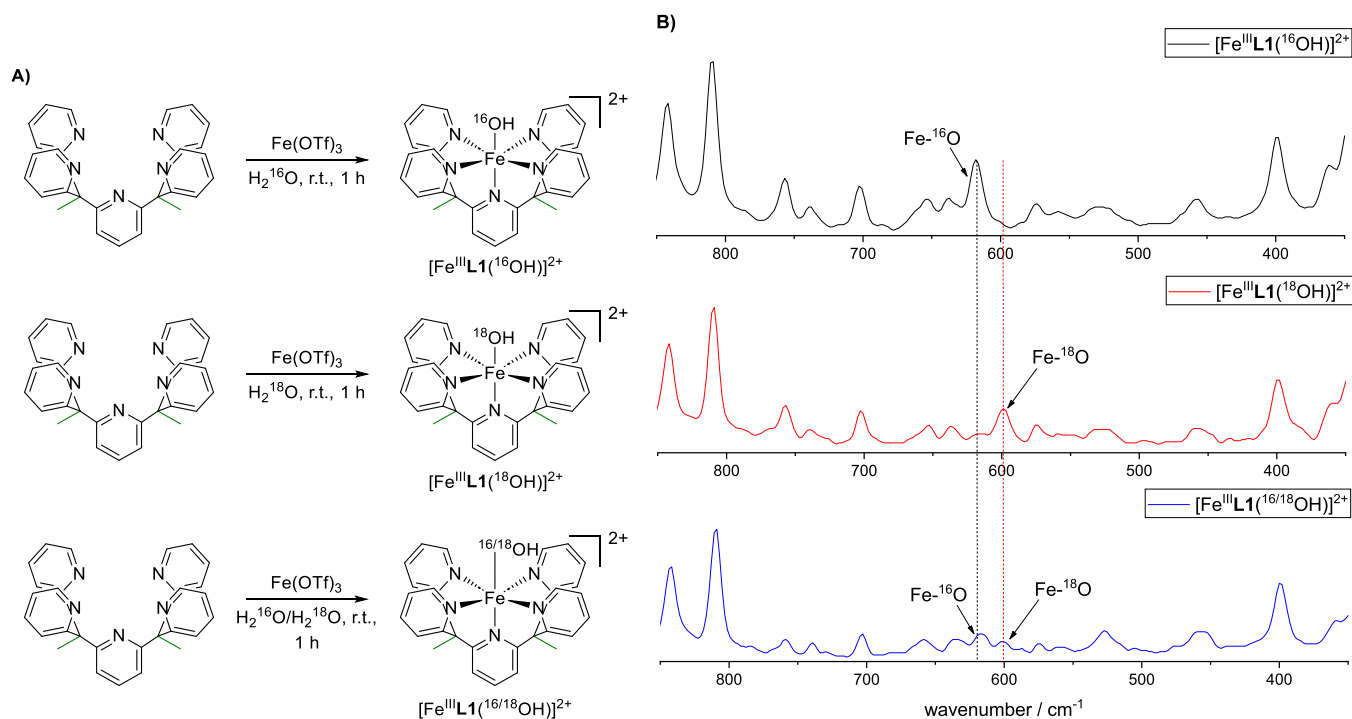


Figure 7. (A) Synthesis of different derivatives of $[\text{Fe}^{\text{III}}\text{L1}(\text{OH})]^{2+}$ from L1: $[\text{Fe}^{\text{III}}\text{L1}^{(16\text{OH})}](\text{OTf})_2$, $[\text{Fe}^{\text{III}}\text{L1}^{(18\text{OH})}](\text{OTf})_2$, and a mixture of $[\text{Fe}^{\text{III}}\text{L1}^{(16/18\text{OH})}](\text{OTf})_2$. (B) Excerpts of solid-state Raman spectra of the corresponding derivatives of $[\text{Fe}^{\text{III}}\text{L1}(\text{OH})]^{2+}$, the respective signal corresponding to the $\text{Fe}-^{16}\text{O}$ or $\text{Fe}-^{18}\text{O}$ bond is indicated.

248 Having observed the L2-based complexes in low-spin
249 electron configurations is so far remarkable, as oxygen-free
250 conditions were used in literature syntheses—a common
251 precaution in the case of high-spin iron complexes. Addition-
252 ally, a low stability was observed in the literature for
253 $[\text{Fe}^{\text{IV}}\text{L2}(\text{O})]^{2+}$, which could have also indicated a high-spin
254 state.³ This was, however, not corroborated by our Mössbauer
255 measurement—even though the samples were handled under
256 ambient conditions for prolonged periods of time.

257 **Characterization of the Iron(III)-Hydroxido Complexes by**
258 **EPR.** The assignment of a low-spin iron(III)-hydroxido species
259 was confirmed by EPR analysis (Figure 6) and subsequent
260 simulation of the assigned low-spin iron(III)-hydroxido
261 compounds. The observed spectra, as well as the observed g
262 values, were qualitatively and quantitatively similar to related

complexes previously described in the literature ($[\text{Fe}^{\text{III}}(\text{PYS})-$
263 $(\text{OMe})]^{2+}$: $g = 2.25, 2.17, 1.96$ and $[\text{Fe}^{\text{III}}(\text{PYS})(\text{OH})]^{2+}$: $g =$
264 $2.30, 2.18, 1.94$ ²; PYS = 2,6-bis(bis(2-pyridyl)-
265 methoxymethane)pyridine).
266

Characterization by High-Resolution Mass Spectrometry
267 **and Raman Spectroscopy.** All iron species were characterized
268 as aqueous solutions with cryo high-resolution mass spectrom-
269 etry (not shown; please refer to the [Figures S53–S58](#), p 36ff).
270 Regarding the iron(III) species $[\text{Fe}^{\text{III}}(\text{L1})(\text{OH})]^{2+}$ or
271 $[\text{Fe}^{\text{III}}(\text{L2})(\text{OH})]^{2+}$, no hints of any bridged diiron(III)
272 complexes have been observed, and no $[\text{Fe}^{\text{III}}(\text{L1})(\text{OH}_2)]^{3+}$
273 or $[\text{Fe}^{\text{III}}(\text{L2})(\text{OH}_2)]^{3+}$ species as potential intermediate were
274 detected. In addition to the expected signals, other minor
275 species could be observed for complexes with the ligand system
276 L2, which were assigned to species such as $[\text{Fe}^{\text{III}}(\text{L2}-$
277

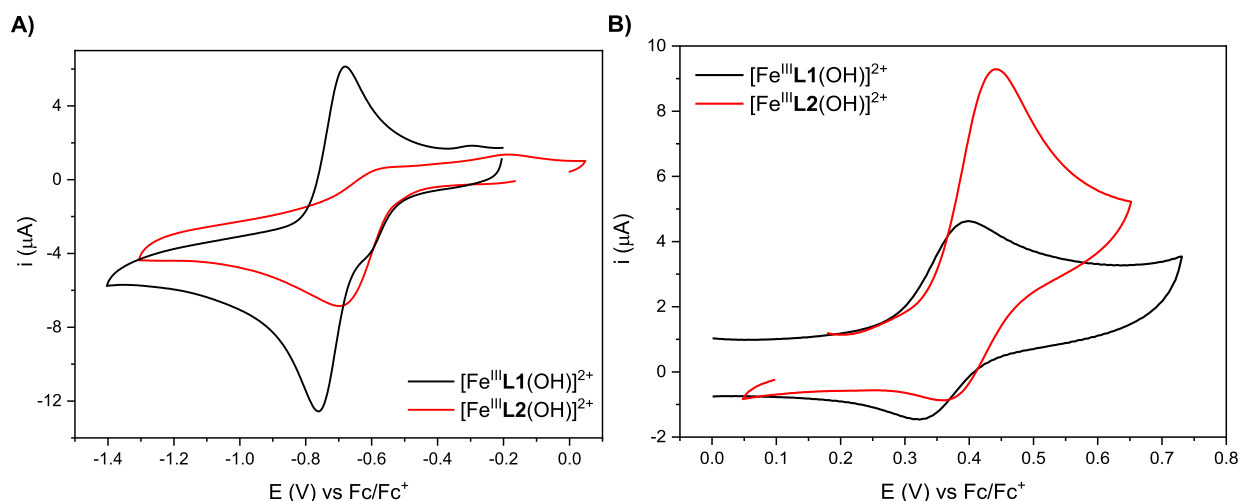


Figure 8. Comparison between the cyclic voltammograms of $[\text{Fe}^{\text{III}}\text{L1}(\text{OH})]^{2+}$ and $[\text{Fe}^{\text{III}}\text{L2}(\text{OH})]^{2+}$ (1 mM) in acetonitrile ($[\text{TBAPF}_6] = 0.1 \text{ M}$) in reductive (A) and oxidative (B) scans at 100 mV/s. For additional cyclic voltammograms, please refer to the Figures S34–S50, p 29ff.

278 $\text{H}(\text{OH})^{2+}$, $[\text{Fe}^{\text{III}}(\text{L2-2H})(\text{OH})]^{2+}$, or dinuclear species
 279 $[\text{Fe}^{\text{II}}(\text{L2-2H})]^{2+}$. This was attributed to a species in which
 280 one or both of the two hydroxy groups of L2 are deprotonated
 281 and likely coordinate to the iron center, probably displacing
 282 one of the equatorial pyridine moieties.

283 We then also synthesized the ^{18}O -labeled derivative of
 284 $[\text{Fe}^{\text{III}}\text{L1}(\text{OH})]^{2+}$ (Figure 7A, middle reaction) as well as a
 285 mixture of $[\text{Fe}^{\text{III}}\text{L1}(^{16}/^{18}\text{OH})]^{2+}$ (Figure 7A, lower reaction).
 286 We confirmed the successful integration of the ^{18}O label by
 287 Raman spectroscopy (Figure 7B). When direct-injection mass
 288 spectrometry of these compounds was measured, only the
 289 species containing the ^{16}OH group could be detected. This
 290 observation was attributed to an immediate exchange of the
 291 hydroxyl group in water. The exchange occurred even when
 292 dried solvents were used under strict inert gas conditions (not
 293 shown).

294 **Characterization by UV–Vis–NIR Spectroscopy.** The
 295 series of complexes was also characterized by UV–vis–NIR
 296 spectroscopy (Figures S31 and S32, p 27f). The UV–vis–NIR
 297 spectra of complexes $[\text{Fe}^{\text{II}}\text{L2}(\text{OH}_2)]^{2+}$, $[\text{Fe}^{\text{III}}\text{L2}(\text{OH})]^{2+}$, and
 298 $[\text{Fe}^{\text{IV}}\text{L2}(\text{O})]^{2+}$ are similar to the respective spectra of
 299 $[\text{Fe}^{\text{II}}\text{L1}(\text{OH}_2)]^{2+}$, $[\text{Fe}^{\text{III}}\text{L1}(\text{OH})]^{2+}$, and $[\text{Fe}^{\text{IV}}\text{L1}(\text{O})]^{2+}$ and
 300 correspond well to those found in the literature.^{47,48} The
 301 absorption maxima at about 350 to 450 nm of the iron(II)
 302 species show the highest intensity, with extinction coefficients
 303 of $\epsilon = 5932/4190 \text{ L mol}^{-1} \text{ cm}^{-1}$ for $[\text{Fe}^{\text{II}}\text{L1}/\text{L2}(\text{OH}_2)]^{2+}$ ($\lambda =$
 304 450 nm, water, 25 °C), which can be attributed to a metal-to-
 305 ligand charge transfer, which has been observed regularly in
 306 literature for iron(II) complexes with pyridine-derived
 307 ligands.^{1–3,8} $[\text{Fe}^{\text{IV}}\text{L2}(\text{O})]^{2+}$ shows an absorption band at $\lambda =$
 308 730 nm, which is a typical range for $S = 1$ iron(IV)-oxido
 309 species.^{8,14,34,42–44}

310 **Characterization by Cyclic Voltammetry.** The redox
 311 properties of the iron(II) and iron(III) complexes (1 mM)
 312 have been addressed by cyclic voltammetry (CV) experiments,
 313 performed both in acetonitrile (using tetrabutylammonium
 314 hexafluorophosphate, $[\text{TBAPF}_6] = 0.1 \text{ M}$ as the supporting
 315 electrolyte) and in aqueous solution (using potassium nitrate,
 316 $[\text{KNO}_3] = 0.1 \text{ M}$ as the supporting electrolyte).

317 In oxidative scan mode in acetonitrile, both iron(II)
 318 complexes present a reversible wave: at 657 mV (vs Fc^+/Fc ,
 319 $\Delta E = 85 \text{ mV}$) and 663 mV (vs Fc^+/Fc , $\Delta E = 76 \text{ mV}$) for

$[\text{Fe}^{\text{II}}\text{L1}(\text{MeCN})]^{2+}$ and $[\text{Fe}^{\text{II}}\text{L2}(\text{MeCN})]^{2+}$, respectively. 320
 These processes are associated with the iron(III)/iron(II) 321
 redox couple (Figures S34–S38, p 29f).⁸ The analogous redox 322
 potential for the two iron(II) centers suggests a negligible 323
 effect associated with the change of the peripheral methyl 324
 group with a hydroxy group.³ 325

Moving to the iron(III) complexes $[\text{Fe}^{\text{III}}\text{L1}(\text{OH})]^{2+}$ and 326
 $[\text{Fe}^{\text{III}}\text{L2}(\text{OH})]^{2+}$, the presence of a negatively charged hydroxy 327
 group directly coordinated to the iron(III) center (instead of 328
 acetonitrile) drastically shifts the potentials of the iron(III)/ 329
 iron(II) redox couples, -720 mV (vs Fc^+/Fc , $\Delta E = 80 \text{ mV}$) 330
 and $E_c^1 = -698 \text{ mV}$ (vs Fc^+/Fc), respectively (Figure 8A). 331
 Contrary to what was previously observed for 332
 $[\text{Fe}^{\text{II}}\text{L1}(\text{MeCN})]^{2+}$ and $[\text{Fe}^{\text{II}}\text{L2}(\text{MeCN})]^{2+}$,^{3,8,47,48} 333
 $[\text{Fe}^{\text{III}}\text{L1}(\text{OH})]^{2+}$ and $[\text{Fe}^{\text{III}}\text{L2}(\text{OH})]^{2+}$ present marked differ- 334
 ences. The iron(III) reduction in $[\text{Fe}^{\text{III}}\text{L2}(\text{OH})]^{2+}$ is shifted to 335
 a more positive potential (approximately 60 mV), and more 336
 importantly, the reoxidation process becomes irreversible 337
 (Figure 8A, see also Figure S40). When the scan rates were 338
 increased, a minor wave at approximately -400 mV was also 339
 observed (Figure S41). Even if the overall process remains 340
 irreversible, this suggests a fast ligand reorganization occurring 341
 after electron transfer (ET). In oxidative scan mode, a new 342
 reversible wave has also been detected for $[\text{Fe}^{\text{III}}\text{L1}(\text{OH})]^{2+}$ at 343
 361 mV (vs Fc^+/Fc , $\Delta E = 76 \text{ mV}$), attributed to the iron(IV)/ 344
 iron(III) redox couple (Figure 8B). $[\text{Fe}^{\text{III}}\text{L2}(\text{OH})]^{2+}$ presents 345
 a similar iron(IV)/iron(III) oxidation potential $E_a^2 = 442 \text{ mV}$, 346
 but the process is again irreversible (Figure 8B). Interestingly, 347
 when the scan rate is gradually increased (Figure S43), a shift 348
 from the initial irreversible wave (100 mV/s) to a quasi- 349
 reversible process ($\Delta E = 100 \text{ mV}$, 600 mV/s) was observed. 350
 This behavior suggests a reversible ET followed by a slow 351
 chemical reaction involving the electrochemically generated 352
 $[\text{Fe}^{\text{IV}}\text{L2}(\text{O})]^{2+}$,⁴⁹ thus indicating a lower stability of 353
 $[\text{Fe}^{\text{IV}}\text{L2}(\text{O})]^{2+}$ compared with $[\text{Fe}^{\text{IV}}\text{L1}(\text{O})]^{2+}$. At higher 354
 potentials, an unresolved irreversible wave at ca. 1.30 V has 355
 also been observed and attributed to a ligand-based oxidation 356
 (refer to the Figures S36, S44, and S45). 357

This suggests how the coordinated OH group in 358
 $[\text{Fe}^{\text{III}}\text{L1}(\text{OH})]^{2+}$ and $[\text{Fe}^{\text{III}}\text{L2}(\text{OH})]^{2+}$ not only contributes 359
 to shifting the iron(III)/iron(II) redox couple to a more 360
 positive potential but also allows access to the iron(IV)-oxido 361

362 state, which is not possible in the absence of an O-donor (see
363 $[\text{Fe}^{\text{II}}\text{L1}(\text{MeCN})]^{2+}$ and $[\text{Fe}^{\text{II}}\text{L2}(\text{MeCN})]^{2+}$ Figures S37 and
364 S38). In addition, the nature of the side CH_3/OH groups
365 seems not to affect the iron redox couple, even if it does impact
366 the stability of the iron(IV) intermediate, as stated above.

367 In unbuffered aqueous media ($[\text{KNO}_3] = 0.1 \text{ M}$),
368 $[\text{Fe}^{\text{III}}\text{L1}(\text{OH})]^{2+}$ presents a quasi-reversible wave in reduction
369 at -6 mV (vs Ag/AgCl , $\Delta E = 144 \text{ mV}$, Figure S46),
370 approximately 300 mV lower in comparison with the potential
371 reported in the literature for the iron(II)– OH_2 species.⁸ An
372 additional minor oxidation wave was observed upon reduction
373 at a potential of approximately 0.20 V (Figures S46 and S47),
374 which was not observed in acetate-buffered solution. Under the
375 same experimental conditions, $[\text{Fe}^{\text{III}}\text{L2}(\text{OH})]^{2+}$ presents a
376 completely different behavior: in the reductive scan, no waves
377 attributable to the presence of an iron(III) center have been
378 observed (Figure S48). In the oxidative scan, a quasi-reversible
379 wave at 372 mV (vs Ag/AgCl , $\Delta E = 111 \text{ mV}$, Figure S49)
380 attributable to the iron(III)/iron(II) redox couple has been
381 observed without the appearance of any additional wave at
382 higher potentials (Figure S50). This suggests the formation of
383 a new iron(II) species from $[\text{Fe}^{\text{III}}\text{L2}(\text{OH})]^{2+}$ under the
384 conditions applied here. This finding prompted us to further
385 study the behavior of this species in solution (vide infra), as we
386 were confident to have obtained a solid iron(III) sample in the
387 first place, as confirmed by EPR and Mössbauer spectroscopy
388 as well as X-ray crystallography.

389 We also investigated the effects of pH changes on the
390 observed potentials of the iron(III)/iron(II) couple of
391 $[\text{Fe}^{\text{III}}\text{L1}(\text{OH})]^{2+}$ and $[\text{Fe}^{\text{II}}\text{L2}(\text{OH}_2)]^{2+}$. Instead of using the
392 iron(II) species $[\text{Fe}^{\text{II}}\text{L1}(\text{OH}_2)]^{2+}$, as had been done previously
393 in the literature,⁸ we used the iron(III)-hydroxido species
394 $[\text{Fe}^{\text{III}}\text{L1}(\text{OH})]^{2+}$ to investigate complexes of L1. We found a
395 linear decrease with a slope value of $-59 \text{ mV}/\text{pH}$, indicating a
396 proton-coupled electron transfer (Figure 9, PCET). In the case

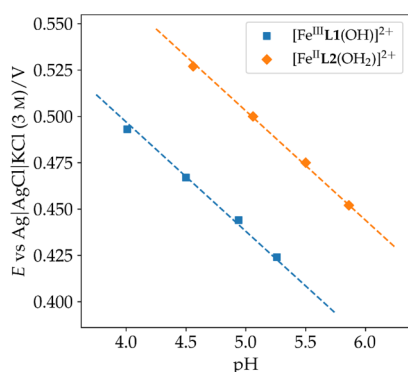


Figure 9. Pourbaix diagram of $[\text{Fe}^{\text{III}}\text{L1}(\text{OH})]^{2+}$ (blue squares) and $[\text{Fe}^{\text{II}}\text{L2}(\text{OH}_2)]^{2+}$ (orange diamonds). The slope values of both lines are $-59 \text{ mV}/\text{pH}$, which indicates a proton-coupled electron transfer (PCET) and was reported for L1 in the literature.⁸

397 of L2, we used the iron(II) complex $[\text{Fe}^{\text{II}}\text{L2}(\text{OH}_2)]^{2+}$ due to
398 its higher stability under prolonged measurements compared
399 with the respective iron(III)-hydroxido complex. The meas-
400 ured values are shifted to higher potentials; however, the slope
401 value is identical at $-59 \text{ mV}/\text{pH}$, also indicating PCET, as has
402 been described in the literature for L1 and other related
403 ligands.^{2,8,50}

404 **Iron(II)/Iron(IV) Comproportionation.** Based on the
405 mechanism proposed for heme and nonheme enzymes

containing iron(IV)-oxido moieties and their reactions with 406
C–H bonds,^{2,8,12,13} we had proposed this iron(III)-hydroxido 407
species as the intermediate in the reaction of $[\text{Fe}^{\text{IV}}\text{L1}(\text{O})]^{2+}$ 408
with organic substrates containing C–H groups in our 409
previous work.⁹ In this mechanism, a hydrogen atom is 410
transferred from the organic substrate R–H to the iron(IV)- 411
oxido moiety in a hydrogen atom transfer reaction (HAT). 412
This step yields the iron(III)-hydroxido species, 413
 $[\text{Fe}^{\text{III}}\text{L1}(\text{OH})]^{2+}$, as well as a carbon-centered radical R·. 414
These species can then recombine in a reaction often referred 415
to as “rebound” to form the product and an iron(II) species in 416
water $[\text{Fe}^{\text{II}}\text{L1}(\text{OH}_2)]^{2+}$ (Figure 10A). This mechanism 417 f10
resembles the consensus mechanism for the oxidation of 418
biological substrates by iron(II)/ α -ketoglutarate-dependent 419
enzymes, of which superfamily the previously mentioned 420
TET enzymes are a member.^{20–23,26,51,52} 421

Surprised by the large amounts of $[\text{Fe}^{\text{III}}\text{L1}(\text{OH})]^{2+}$ present 422
in the reaction mixture of $[\text{Fe}^{\text{IV}}\text{L1}(\text{O})]^{2+}$ and SmC (Figure 11) 423 f11
after complete reaction, we searched for different pathways 424
that might lead to the formation of this iron(III)-hydroxido 425
species. 426

For synthetic nonheme iron complexes, several other 427
mechanisms and pathways are discussed in addition to 428
rebound: cage escape³³ and the formation of a dinuclear 429
complex, as mentioned in the introduction,¹⁴ are two 430
representatives. Also, comproportionation of iron(II)/iron(IV) 431
species has been described in the literature, although mostly as 432
a minor side-note.^{14,31,53} In the case of the complexes studied 433
in this work, we found that the comproportionation reaction of 434
 $[\text{Fe}^{\text{II}}\text{L1}(\text{OH}_2)]^{2+}$ with $[\text{Fe}^{\text{IV}}\text{L1}(\text{O})]^{2+}$ gave $[\text{Fe}^{\text{III}}\text{L1}(\text{OH})]^{2+}$ in 435
a quantitative yield. The UV–vis–NIR spectrum of an 436
equimolar mixture of $[\text{Fe}^{\text{II}}\text{L1}(\text{OH}_2)]^{2+}$ and $[\text{Fe}^{\text{IV}}\text{L1}(\text{O})]^{2+}$ 437
appears to have identical features compared to the spectrum 438
of a $[\text{Fe}^{\text{III}}\text{L1}(\text{OH})]^{2+}$ reference sample (Figure 12). This 439 f12
observation was also confirmed by cryo-UHR–MS (refer to 440
Figure S59, p 43). Whereas Gosh et al.²⁹ and Rana et al.⁵³ 441
report on the comproportionation of biuret-amide and N4P- 442
based systems, respectively, Cho et al. ruled out comproportion- 443
ation when studying $[\text{Fe}^{\text{IV}}(\text{O})(\text{Bn-TPEN})]^{2+}$ (Bn-TPEN = 444
N-benzyl-*N,N',N'*-tris(2-pyridylmethyl)ethane-1,2-diamine). 445
In this work, we report on another example of the 446
comproportionation of iron(IV)-oxido and iron(II) com- 447
pounds as a pathway for synthetic nonheme iron(IV)-oxido 448
complexes. 449

As a result, we decided to study this behavior in more detail 450
and chose to include the iron complexes of the structurally 451
similar ligand L2 in this analysis. We found that not only 452
 $[\text{Fe}^{\text{II}}\text{L1}(\text{OH}_2)]^{2+}$ and $[\text{Fe}^{\text{IV}}\text{L1}(\text{O})]^{2+}$ but also 453
 $[\text{Fe}^{\text{II}}\text{L2}(\text{OH}_2)]^{2+}$ and $[\text{Fe}^{\text{IV}}\text{L2}(\text{O})]^{2+}$ show comproportiona- 454
tion behavior—as well as the cross-reactions of 455
 $[\text{Fe}^{\text{II}}\text{L1}(\text{OH}_2)]^{2+}$ with $[\text{Fe}^{\text{IV}}\text{L2}(\text{O})]^{2+}$ and $[\text{Fe}^{\text{II}}\text{L2}(\text{OH}_2)]^{2+}$ 456
with $[\text{Fe}^{\text{IV}}\text{L1}(\text{O})]^{2+}$, the latter two giving a mixture of 457
 $[\text{Fe}^{\text{III}}\text{L1}(\text{OH})]^{2+}$ and $[\text{Fe}^{\text{III}}\text{L2}(\text{OH})]^{2+}$. The iron(II) species 458
 $[\text{Fe}^{\text{II}}\text{L1}(\text{OH}_2)]^{2+}$ and $[\text{Fe}^{\text{II}}\text{L2}(\text{OH}_2)]^{2+}$ as well as the iron(IV)- 459
oxido complexes $[\text{Fe}^{\text{IV}}\text{L1}(\text{O})]^{2+}$ and $[\text{Fe}^{\text{IV}}\text{L2}(\text{O})]^{2+}$ do not 460
react with each other; both reactions were observed to yield a 461
mixture of the respective starting materials. 462

To gain a deeper insight into this reactivity, these individual 463
comproportionation reactions were followed by stopped-flow 464
UV–vis–NIR kinetics (Figure 13). The presence of both 465 f13
iron(II) and iron(IV)-oxido complexes was measured at the 466
respective absorption maxima ($[\text{Fe}^{\text{II}}\text{L1}(\text{OH}_2)]^{2+}/$ 467

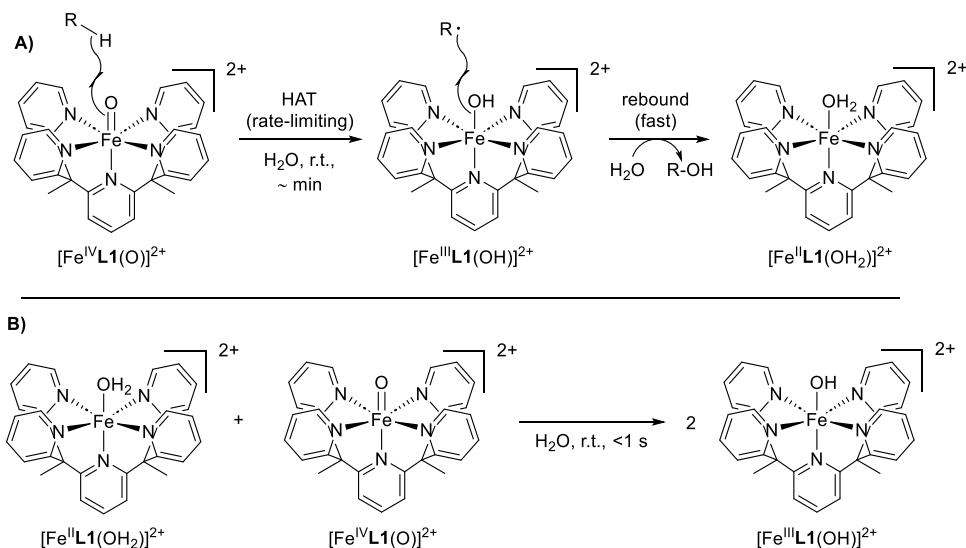
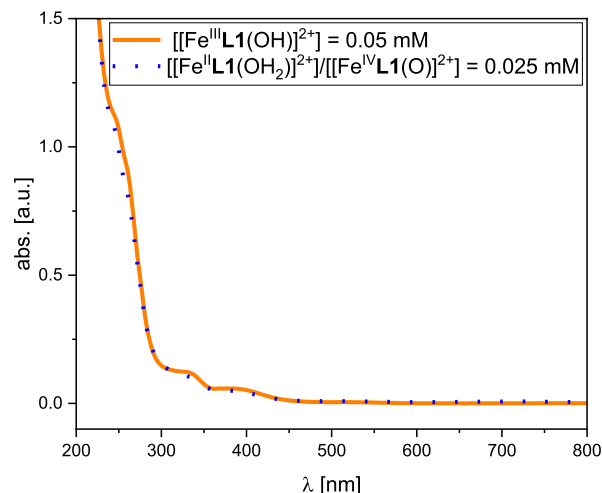
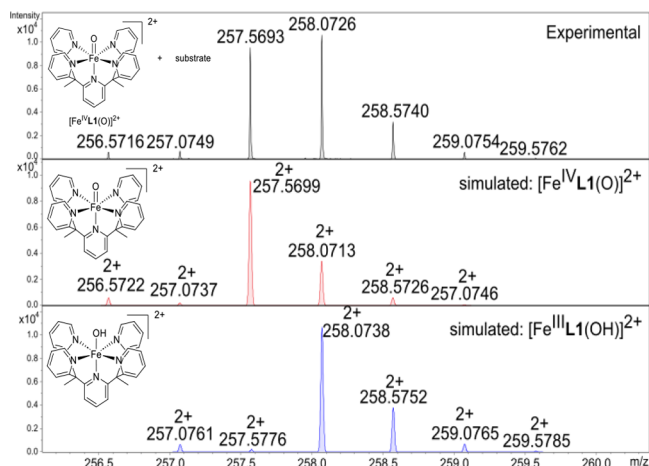


Figure 10. (A) Proposed mechanism for the reaction of $[\text{Fe}^{\text{IV}}\text{L1}(\text{O})]^{2+}$ with an organic substrate R-H that contains a C–H bond via hydrogen atom transfer (HAT) and subsequent rebound.⁹ (B) Observed comproportionation reaction of the iron(II) complex $[\text{Fe}^{\text{II}}\text{L1}(\text{OH}_2)]^{2+}$ and the iron(IV)-oxido complex $[\text{Fe}^{\text{IV}}\text{L1}(\text{O})]^{2+}$ to yield iron(III)-hydroxido species $[\text{Fe}^{\text{III}}\text{L1}(\text{OH})]^{2+}$.



468 $[\text{Fe}^{\text{II}}\text{L2}(\text{OH}_2)]^{2+}$; $\lambda = 450 \text{ nm}$, $[\text{Fe}^{\text{IV}}\text{L1}(\text{O})]^{2+}$; $\lambda = 720 \text{ nm}$,
469 and $[\text{Fe}^{\text{IV}}\text{L2}(\text{O})]^{2+}$; $\lambda = 730 \text{ nm}$).

470 A comparison of the decreasing absorption of both iron(II)
471 and iron(IV)-oxido species over time suggests a bimolecular
472 reaction of both complexes (not shown; please refer to the
473 Figure S4, p 10). Using the same analytical kinetics we applied
474 to study the reaction of $[\text{Fe}^{\text{IV}}\text{L1}(\text{O})]^{2+}$ with organic substrates
475 in our previous work,¹¹ we obtained rate constants in the order
476 of $1.5\text{--}4.2 \times 10^4 \text{ L mol}^{-1} \text{ s}^{-1}$ (refer to the Supporting
477 Information, p 9f for detailed calculations.) These values are
478 4–6 orders of magnitude larger than those observed for
479 $[\text{Fe}^{\text{IV}}\text{L1}(\text{O})]^{2+}$ with a variety of alkyl group-bearing substrates,
480 both the ones tested in this work (vide infra) and in our
481 previous work.¹¹

482 The stopped-flow UV-vis-NIR measurements were
483 repeated in deuterated water, and the same linear regression
484 calculations were performed. A kinetic isotope effect (KIE) was
485 observed in the range of 1.9 to 5.6, which would suggest a
486 proton transfer to be the rate-limiting step in this reaction.

487 Interestingly, this isotope effect seems to be more pronounced
488 in comproportionation reactions involving iron complexes with
489 the ligand system L2. A comparison of all conducted
490 measurements in water or deuterated water is provided in
491 the Figures S4–S6, p 11ff.

492 **Substrate Oxidation by Iron(IV)-Oxido Species.** In the
493 next step, we wanted to confirm the oxidative capabilities of
494 $[\text{Fe}^{\text{IV}}\text{L2}(\text{O})]^{2+}$ and compare the reactivities of the two
495 different ligand systems in substrate oxidation processes.
496 Therefore, complexes $[\text{Fe}^{\text{IV}}\text{L1}(\text{O})]^{2+}$ and $[\text{Fe}^{\text{IV}}\text{L2}(\text{O})]^{2+}$
497 were reacted with selected substrates chosen on the basis of
498 the work of Chantarojsiri et al.⁸ (Chart 2). Due to the high
499 reactivity of the iron(IV)-oxido complexes toward organic
500 substrates, no organic buffers could be used. Due to solubility
501 issues in phosphate buffer, pure water was chosen. The pH
502 value after the addition of all components was measured at 502

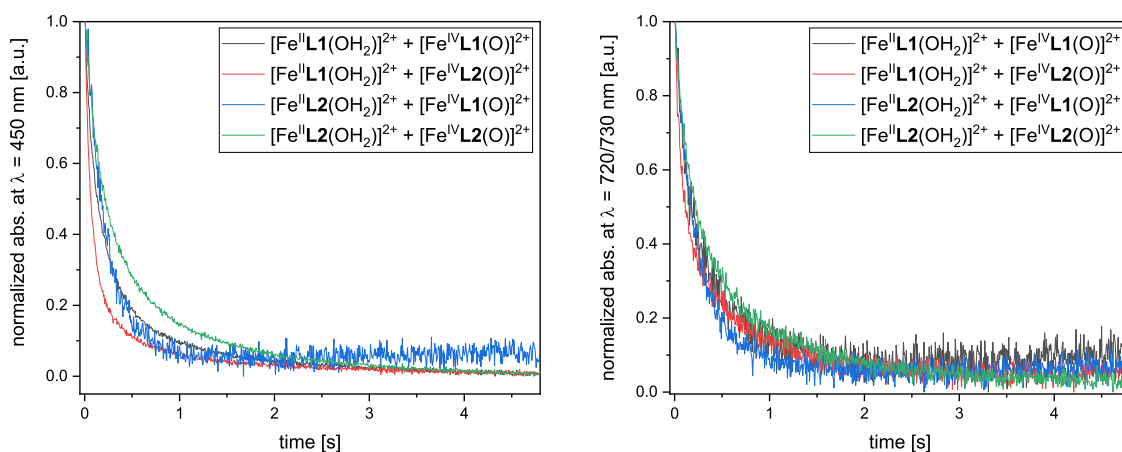
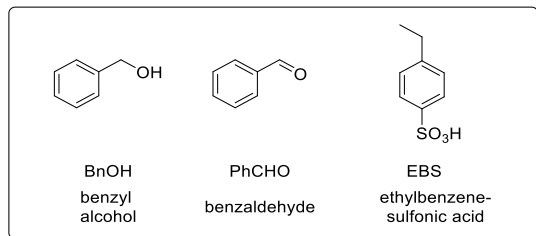


Figure 13. Equimolar reaction of iron(II) and iron(IV)-oxido species followed by stopped-flow UV-vis-NIR spectroscopy at the respective absorption band (iron(II): $\lambda = 450$ nm; iron(IV): $\lambda = 720/730$ nm). Conditions: $[[\text{Fe}^{\text{II}}\text{L1}(\text{OH}_2)]^{2+} \text{ or } [\text{Fe}^{\text{II}}\text{L2}(\text{OH}_2)]^{2+}] = [[\text{Fe}^{\text{IV}}\text{L1}(\text{O})]^{2+} \text{ or } [\text{Fe}^{\text{IV}}\text{L2}(\text{O})]^{2+}] = 0.5$ mM, H_2O , 25°C .

Chart 2. Overview of Substrates (S) Tested in the Reactivity Study



synthesized $[\text{Fe}^{\text{IV}}\text{L2}(\text{O})]^{2+}$ reacts slightly faster with the substrates benzyl alcohol ($10.94 \text{ L mol}^{-1} \text{ s}^{-1}$) and ethylbenzenesulfonic acid ($16.75 \text{ L mol}^{-1} \text{ s}^{-1}$) than the literature-known compound $[\text{Fe}^{\text{IV}}\text{L1}(\text{O})]^{2+}$ (7.40 and $11.99 \text{ L mol}^{-1} \text{ s}^{-1}$, respectively). In the case of benzaldehyde, no significant difference in reaction rates could be observed ($2.08 \text{ L mol}^{-1} \text{ s}^{-1}$ for $[\text{Fe}^{\text{IV}}\text{L2}(\text{O})]^{2+}$ and $2.77 \text{ L mol}^{-1} \text{ s}^{-1}$ for $[\text{Fe}^{\text{IV}}\text{L1}(\text{O})]^{2+}$; Figure 14B). The faster reaction of both iron complexes with benzyl alcohol as the substrate compared to benzaldehyde is in accordance with the reactivity expected from the corresponding C-H bond dissociation energies of the substrates ($83.0 \text{ kcal mol}^{-1}$ for benzyl alcohol⁵⁴ and $89.3 \text{ kcal mol}^{-1}$ for benzaldehyde⁵⁵). Hydrogen atom transfer occurs faster with lower BDE, and this observation supports the reaction mechanism proposed in Figure 10.

To ensure that substrate oxidation occurred, the products after the reaction with the iron(IV)-oxido species were identified by ^1H NMR spectroscopy. In the case of benzyl alcohol and benzaldehyde, this was accomplished by extracting the aqueous reaction mixture with deuterated chloroform, leaving the remaining iron species in the aqueous layer. As

4.77 \pm 0.10 at the beginning of the reaction and found to decrease to 4.68 during the reaction (refer to the Figure S2, p 7 for details).

The reaction was followed with UV-vis-NIR spectroscopy at the characteristic iron(IV)-oxido absorption band ($\lambda = 720$ nm for $[\text{Fe}^{\text{IV}}\text{L1}(\text{O})]^{2+}$ and $\lambda = 730$ nm for $[\text{Fe}^{\text{IV}}\text{L2}(\text{O})]^{2+}$), which decreases during the reaction as the iron(IV)-oxido species is consumed (Figure 14A). The reaction rates were calculated using the method of initial rates. The newly

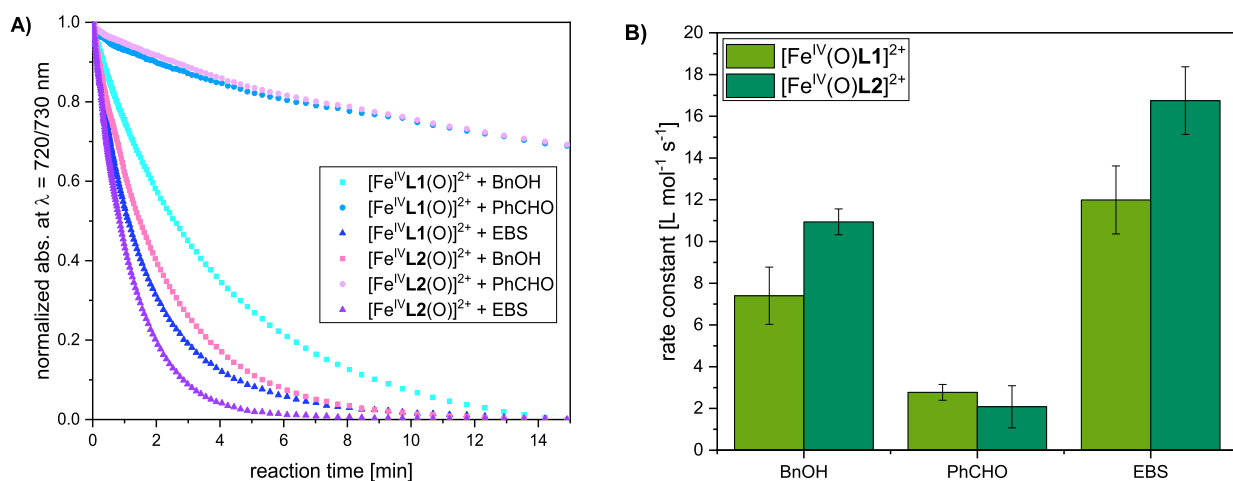


Figure 14. (A) Reaction of $[\text{Fe}^{\text{IV}}\text{L1}(\text{O})]^{2+}$ and $[\text{Fe}^{\text{IV}}\text{L2}(\text{O})]^{2+}$ with different substrates monitored by UV-vis-NIR absorption at $\lambda = 720$ nm ($[\text{Fe}^{\text{IV}}\text{L1}(\text{O})]^{2+}$) or $\lambda = 730$ nm ($[\text{Fe}^{\text{IV}}\text{L2}(\text{O})]^{2+}$) and (B) calculated rate constants for these reactions (refer to the literature¹¹ and the Supporting Information, p 7 for calculation method, exact values, and comparison with corresponding BDE values). Conditions: $[[\text{Fe}^{\text{IV}}\text{L1}(\text{O})]^{2+} / [\text{Fe}^{\text{IV}}\text{L2}(\text{O})]^{2+}] = [\text{S}] = 0.5$ mM, H_2O , rt. The experiments were conducted in triplicate and averaged.

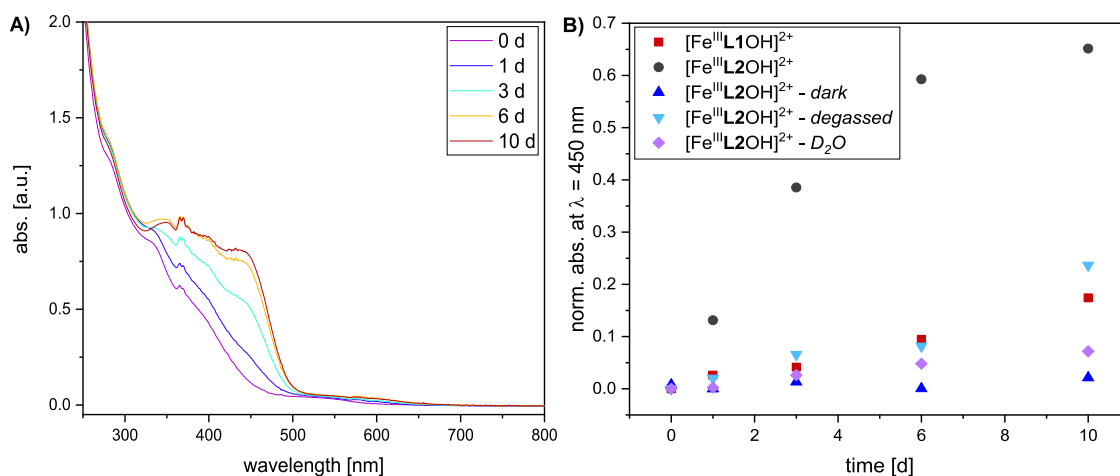


Figure 15. (A) UV–vis–NIR spectra of $[\text{Fe}^{\text{III}}\text{L2}(\text{OH})]^{2+}$ in aqueous solution under ambient conditions and exposed to light after different times and (B) absorbance of $[\text{Fe}^{\text{III}}\text{L1}(\text{OH})]^{2+}$ and $[\text{Fe}^{\text{III}}\text{L2}(\text{OH})]^{2+}$ at $\lambda = 450$ nm over time. Conditions: $[[\text{Fe}^{\text{III}}\text{L1}(\text{OH})]^{2+}$ or $[\text{Fe}^{\text{III}}\text{L2}(\text{OH})]^{2+}] = 0.5$ mM, H_2O , 25 °C. Additional spectra are provided in the Figure S33, p 28.

533 expected, benzyl alcohol was first converted into benzaldehyde,
 534 which reacted further to benzoic acid (Figures S15–S18). As
 535 the substrate ethylbenzenesulfonic acid (EBS) remained in the
 536 aqueous layer, this method could not be applied here. To
 537 separate the formed products from the iron species present, the
 538 yellowish reaction mixture was filtered over silica. The yellow
 539 iron species remained on the silica, and the clear filtrate was
 540 analyzed with ^1H NMR spectroscopy (Figures S27 and S28).
 541 In addition to the EBS starting material, two new species could
 542 be observed, which were attributed to the hydroxylated (4-(1-
 543 hydroxyethyl)benzenesulfonic acid) and carbonylated (4-
 544 acetylbenzenesulfonic acid) derivative of EBS. LC–MS
 545 measurements support this assumption (Figures S64 and
 546 S65, p 46). Control reactions with the corresponding iron(II)
 547 or iron(III) species revealed no oxidation of the substrates
 548 under the applied conditions (please refer to the Figures S19–
 549 S26 and S29, p 21ff). The results presented herein show that
 550 the complex with L2 is a suitable model system for further
 551 investigations of iron-dependent nonheme enzymes, just as
 552 $[\text{Fe}^{\text{IV}}\text{L1}(\text{O})]^{2+}$ has been used in recent years as a model
 553 system.^{9–11} The observed difference in reaction rates with
 554 organic substrates might offer intriguing possibilities for
 555 differential oxidation of several substrates in the same reaction
 556 mixture, depending on the added iron catalyst, mimicking
 557 complex enzyme mixtures in living cells.

558 **Iron(III) to Iron(II) Conversion.** Puzzled by the detection
 559 of iron(II) species upon the application of iron(III) species in
 560 some cyclic voltammetry experiments, a possible reduction of
 561 iron(III) under the applied conditions was assumed. To test
 562 the stability of the iron(III) species in aqueous solution, UV–
 563 vis–NIR spectra of $[\text{Fe}^{\text{III}}\text{L1}(\text{OH})]^{2+}$ and $[\text{Fe}^{\text{III}}\text{L2}(\text{OH})]^{2+}$
 564 were recorded at certain time intervals (see Figure 15).

565 The UV–vis–NIR spectra show that when $[\text{Fe}^{\text{III}}\text{L2}(\text{OH})]^{2+}$
 566 is stored in aqueous solution at ambient conditions, a new
 567 absorption band is formed after some time (Figure 15A). The
 568 higher intensity and position of this new absorption band
 569 (about $\lambda = 450$ nm) suggest the formation of the
 570 corresponding iron(II) species. To test this hypothesis, a
 571 sample of $[\text{Fe}^{\text{III}}\text{L2}(\text{OH})]^{2+}$ in water was kept under ambient
 572 conditions for 5 weeks, the solvent was removed, and the
 573 sample was subjected to Mössbauer measurements. The
 574 spectra revealed that 37% of the iron(III) species has been

575 converted into an iron(II) species (not shown; please refer to
 576 the Figure S67, p 47). The parameters of the newly observed
 577 species are similar but not identical to the iron(II)/iron(III)
 578 reference samples (see Table S6, p 47), and this slight
 579 difference is attributed to the assumed presence of water as a
 580 co-ligand for the iron(II) species (instead of acetonitrile) and
 581 possible ligand oxidation for both species. The complex with
 582 the other ligand system $[\text{Fe}^{\text{III}}\text{L1}(\text{OH})]^{2+}$ showed similar
 583 behavior, but the transformation occurred significantly slower
 584 (Figure 15B).

585 To learn more about this process, three different aqueous
 586 solutions of $[\text{Fe}^{\text{III}}\text{L2}(\text{OH})]^{2+}$ were prepared (a) with exclusion
 587 of light, (b) under a nitrogen atmosphere using degassed water,
 588 and (c) under ambient conditions but using deuterated water.
 589 Light exclusion led to no conversion to iron(II) species over
 590 the investigated time, and with the exclusion of oxygen, the
 591 transformation started slower and not immediately (Figure
 592 15B). As no other suitable reaction partner is present in the
 593 reaction mixture, we assume that in combination with the
 594 reduction from iron(III) to iron(II) species, oxidation of the
 595 ligand occurs. It seems that light is required to start this
 596 oxidation process, which indicates the involvement of one-
 597 electron processes. This has been described previously in the
 598 literature, e.g., a tpena-based iron(III) complex (tpena =
 599 N,N,N' -tris(2-pyridylmethyl)ethylendiamine- N' -acetate) was
 600 reported to photolytically release CO_2 in a one-electron
 601 reduction to the respective iron(II) complex with a radical
 602 present on the ligand.⁵⁶ Then, traces of oxygen seem to be
 603 sufficient for the conversion to occur. When $[\text{Fe}^{\text{III}}\text{L2}(\text{OH})]^{2+}$
 604 is dissolved in deuterated water instead of water under ambient
 605 conditions, no conversion into the iron(II) species is observed
 606 over the investigated time (Figure 15B), suggesting that proton
 607 transfer also seems to play a role in this transformation process.

608 These findings show that after the comproportionation of
 609 iron(II) and iron(IV) species, the resulting iron(III)
 610 compound seems not to be the final product in this complex
 611 mixture. Even though magnitudes of dimensions lie between
 612 the reaction rates of these two different processes (seconds for
 613 the comproportionation and days/weeks for iron(III) to
 614 iron(II) conversion), it appears that, in the end, the most
 615 stable species is an iron(II) complex under the conditions
 616 applied here.

617 ■ CONCLUSIONS

618 In this work, we presented a comprehensive overview of the
619 iron(II), iron(III)-hydroxido, and iron(IV)-oxido chemistry of
620 two pentapyridyl ligands, L1 and L2. With the exception of
621 $[\text{Fe}^{\text{IV}}\text{L2}(\text{O})]^{2+}$, we provided a full set of X-ray structures for all
622 three oxidation states for both ligands, including the relatively
623 rare low-spin iron(III)-hydroxido complexes, $[\text{Fe}^{\text{III}}\text{L1}(\text{OH})]^{2+}$
624 and $[\text{Fe}^{\text{III}}\text{L2}(\text{OH})]^{2+}$. We complemented these X-ray
625 structures with further structural investigations using Mössbauer,
626 EPR, as well as UV–vis–NIR and IR spectroscopy, and
627 the electrochemistry of the iron compounds was studied with
628 cyclic voltammetry investigations. Additionally, UV–vis–NIR
629 kinetic analysis of the reactivity of the iron(IV)-oxido
630 compounds, $[\text{Fe}^{\text{IV}}\text{L1}(\text{O})]^{2+}$ and $[\text{Fe}^{\text{IV}}\text{L2}(\text{O})]^{2+}$, toward a
631 series of substrates was performed. Thereby, we could establish
632 a structure–function relationship between the methyl group in
633 L1-derived compounds and the hydroxyl group in L2-derived
634 compounds. The comproportionation reaction of iron(II)
635 compounds $[\text{Fe}^{\text{II}}\text{L1}(\text{OH}_2)]^{2+}$ and $[\text{Fe}^{\text{II}}\text{L2}(\text{OH}_2)]^{2+}$ with
636 iron(IV)-oxido complexes $[\text{Fe}^{\text{IV}}\text{L1}(\text{O})]^{2+}$ and $[\text{Fe}^{\text{IV}}\text{L2}(\text{O})]^{2+}$
637 was confirmed using UV–vis–NIR spectroscopy and high-
638 resolution mass spectrometry. This finding is especially
639 relevant for the bioinorganic chemistry of these complexes,
640 as it shows that iron model systems of enzymes do undergo
641 significant side reactions.

642 ■ EXPERIMENTAL SECTION

643 **Synthesis of 2,2'-(ethane-1,1'diyl)dipyridine (1).** According
644 to a modified literature procedure,⁵⁷ a flame-dried flask was charged
645 with 2-ethylpyridine (6.27 mL, 5.88 g, 54.84 mmol, 2.1 equiv) under
646 an inert atmosphere (nitrogen) and 50 mL of absolute tetrahydrofuran
647 an and then cooled to -78°C . When a solution of *n*-butyl lithium
648 (2.5 M in hexane, 20.80 mL, 52.01 mmol, 2.0 equiv) was added
649 dropwise, the solution turned deep red. The mixture was stirred for 60
650 min at -78°C , and then 2-fluoropyridine (2.21 mL, 2.50 g, 25.8
651 mmol, 1.0 equiv) was added dropwise; the solution was stirred at -78°C
652 $^\circ\text{C}$ for an additional 10 min, and the cooling bath was removed. The
653 reaction mixture was allowed to warm to room temperature and then
654 stirred at room temperature for 3 h. Next, 30 g of ice was added
655 slowly, at which point the mixture turned yellow. An additional 30 mL
656 of Milli-Q grade water was added, and the solution was stirred
657 vigorously for 10 min. The layers were separated, and the aqueous
658 layer was extracted with dichloromethane (3×50 mL). The
659 combined organic layers were dried over anhydrous magnesium
660 sulfate, and the solvents were removed in vacuo to yield a yellow to
661 orange oil as the crude product. Excess 2-ethylpyridine was removed
662 under reduced pressure to yield product 1 as a yellow to orange oil in
663 84% yield (3.79 g). $R_F = 0.23$ (silica, UV, 80% ethyl acetate -
664 hexanes). $^1\text{H NMR}$ (400.0 MHz, CDCl_3 , 295 K): $\delta = 8.55$ (ddd, $J =$
665 4.9 Hz, $J = 1.9$ Hz, $J = 0.9$ Hz, 2H), 7.60 (td, $J = 7.7$ Hz, $J = 1.8$ Hz,
666 2H), 7.28 (dd, $J = 7.9$ Hz, $J = 1.0$ Hz, 2H), 7.11 (ddd, $J = 7.5$ Hz, $J =$
667 4.9 Hz, $J = 1.2$ Hz, 2H), 4.48 (q, $J = 7.2$ Hz, 2H), 1.76 (d, $J = 7.2$ Hz,
668 3H) ppm. $^{13}\text{C NMR}$ (100.0 MHz, CDCl_3 , 295 K): $\delta = 163.9$, 149.3,
669 136.6, 122.5, 121.5, 49.9, 19.8 ppm. NMR data are in accordance with
670 the literature.⁵⁷ **HR–MS (ESI):** Calculated for $\text{C}_{12}\text{H}_{13}\text{N}_2$ $[\text{M} + \text{H}]^+$:
671 185.10787 m/z ; Found: 185.10723 m/z .

672 **Synthesis of L1.** According to a modified literature procedure,^{8,9} a
673 flame-dried flask was charged with 1 (2.00 g, 10.9 mmol, 3.0 equiv),
674 36 mL of absolute 1,4-dioxane under an inert atmosphere (nitrogen),
675 and 4 mL of absolute tetrahydrofuran and cooled to 0°C . When a
676 solution of *n*-butyl lithium (2.5 M in hexane, 4.34 mL, 10.9 mmol, 3.0
677 equiv) was added, the solution turned dark red. The solution was
678 stirred for 45 min at 0°C , at which time 2,6-dichloropyridine (535.5
679 mg, 3.62 mmol, 1.0 equiv) was added all at once. The reaction
680 mixture was allowed to warm to room temperature and then heated to
681 reflux for 60 h (bath temperature 105°C). When the solution had

turned from deep red to light brown and thin-layer chromatography 682
showed no change during a time span of 6 h, the mixture was allowed 683
to cool to room temperature. Then, 20 mL of water was added, and 684
the mixture was extracted with dichloromethane (3×70 mL). The 685
combined organic layers were then dried over anhydrous magnesium 686
sulfate, and the solvents were removed in vacuo. Afterward, 40 mL of 687
methanol was added, and the solvents were removed in vacuo to 688
remove residual 1,4-dioxane. A deep red oil was obtained as the crude 689
product. Diethyl ether was added until a yellow precipitate began to 690
form, which was filtered off, washed with diethyl ether (1×10 mL), 691
and dried to yield the product L1 as a yellow solid in 91% yield. $R_F =$ 692
0.10 (silica, UV, 80% ethyl acetate - hexanes). $^1\text{H NMR}$ (400.0 MHz, 693
 CDCl_3 , 295 K): $\delta = 8.51$ (ddd, $J = 4.8$ Hz, $J = 1.9$ Hz, $J = 0.9$ Hz, 4H), 694
7.54 (t, $J = 7.9$ Hz, 1H), 7.39 (ddd, $J = 8.1$ Hz, $J = 7.5$ Hz, $J = 1.9$ Hz, 695
4H), 7.05 (d, $J = 7.9$ Hz, 2H) 7.04 (ddd, $J = 7.5$ Hz, $J = 4.8$ Hz, $J =$ 696
1.1 Hz, 4H), 6.84 (dt, $J = 8.0$ Hz, $J = 1.0$ Hz, 4H), 2.21 (s, 6H) ppm. 697
 $^{13}\text{C NMR}$ (100.0 MHz, CDCl_3 , 295 K): $\delta = 166.2$, 166.3, 148.5, 698
136.8, 135.6, 124.1, 121.0, 120.0, 60.1, 26.8 ppm. NMR data are in 699
accordance with the literature.⁸ **HR–MS (ESI):** Calculated for 700
 $\text{C}_{29}\text{H}_{26}\text{N}_5$ $[\text{M} + \text{H}]^+$: 444.21882 m/z ; Found: 444.21811 m/z . **IR** 701
(**thin film**): $\nu = 3053$, 2992, 1566, 1466, 1428, 1365, 1293, 1153, 702
1102, 1078, 1067, 1046, 991, 962, 903, 875, 799, 786, 768, 752, 699, 703
654 cm^{-1} . 704

Synthesis of $[\text{Fe}^{\text{II}}\text{L1}(\text{MeCN})](\text{OTf})_2$. According to a modified 705
literature procedure,^{8,9} ligand L1 (300.0 mg, 0.679 mmol, 1.0 equiv) 706
was dissolved in 15 mL of acetonitrile under a nitrogen atmosphere. 707
Iron(II)bis(acetonitrile)bis(triflate) (294.9 mg, 0.679 mmol, 1.0 708
equiv) was added as a solid, turning the solution deep red. The 709
mixture was then stirred for an additional 5 min, and then diethyl 710
ether was diffused into the solution under ambient conditions to give 711
the product $[\text{Fe}^{\text{II}}\text{L1}(\text{MeCN})](\text{OTf})_2$ as brown crystals in 91% yield 712
(516.0 mg). $^1\text{H NMR}$ (400.0 MHz, CD_3CN , 295 K): $\delta = 9.81$ (d, $J =$ 713
5.9 Hz, 4H), 8.03 (s, 3H), 7.93 (d, $J = 3.8$ Hz, 8H), 7.54 (m, 4H), 714
2.75 (s, 6H), 1.96 (s, 3H) ppm. $^{13}\text{C NMR}$ (100.0 MHz, CD_3CN , 295 715
K): $\delta = 165.0$, 163.0, 158.2, 140.1, 139.7, 124.3, 123.8, 122.1, 118.3, 716
55.7, 24.2 ppm. NMR data are in accordance with the literature.⁸ **HR–** 717
MS (ESI): Calculated for $\text{C}_{30}\text{H}_{25}\text{F}_3\text{FeN}_5\text{O}_3\text{S}$ $[\text{Fe}(\text{L1})(\text{MeCN})-$ 718
 $(\text{OTf})]^+$: 648.09796 m/z ; Found: 648.09648 m/z . Calculated for 719
 $\text{C}_{31}\text{H}_{28}\text{FeN}_6$ $[\text{Fe}(\text{L1})(\text{MeCN})]^{2+}$: 270.08625 m/z ; Found: 270.08562 720
 m/z . **Elemental Analysis:** Calculated for $\text{C}_{33}\text{H}_{28}\text{F}_6\text{FeN}_6\text{O}_6\text{S}_2$: C 721
47.27, H 3.37, N 10.02, S 7.65; Found: C 47.03, H 3.33, N 9.94, S 722
7.86. **IR (thin film):** $\nu = 1598$, 1469, 1442, 1415, 1281, 1251, 1225, 723
1149, 1070, 1028, 865, 791, 761, 702 cm^{-1} . 724

Synthesis of $[\text{Fe}^{\text{II}}\text{L1}(\text{OH}_2)](\text{BF}_4)_2$. According to a modified 725
literature procedure,⁸ ligand L1 (90.0 mg, 0.190 mmol, 1.0 equiv) 726
was dissolved in 4.0 mL of acetone. Hexaqua iron(II) bis- 727
(tetrafluoroborate) (64.2 mg, 0.190 mmol, 1.0 equiv) was dissolved 728
in 0.5 mL of water and then added to the solution of the ligand, 729
turning the solution red-brown. The mixture was stirred for 5 min, 730
and then diethyl ether was diffused into the solution to give the 731
product $[\text{Fe}^{\text{II}}\text{L1}(\text{OH}_2)](\text{OTf})_2$ as a red-brown powder in 73% yield 732
(100.0 mg). **HR–MS (ESI):** Calculated for $\text{C}_{29}\text{H}_{25}\text{FFeN}_5$ $[\text{Fe}(\text{L1})-$ 733
 $(\text{F})]^+$: 518.14434 m/z ; Found: 518.14454 m/z . Calculated for 734
 $\text{C}_{31}\text{H}_{28}\text{FeN}_6$ $[\text{Fe}(\text{L1})(\text{MeCN})]^{2+}$: 270.08625 m/z ; Found: 735
270.05525 m/z . Calculated for $\text{C}_{31}\text{H}_{28}\text{FeN}_6$ $[\text{Fe}(\text{L1})]^{2+}$: 249.5730 736
 m/z ; Found: 249.5730 m/z . **Elemental Analysis:** Calculated for 737
 $\text{C}_{29}\text{H}_{27}\text{B}_2\text{F}_8\text{FeN}_5\text{O}$: C 50.41, H 3.94, N 10.15; Found: C 50.43, H 738
3.80, N 10.11. **IR (thin film):** $\nu = 3398$, 1653, 1597, 1465, 1442, 739
1412, 1390, 1283, 1069, 993, 863, 768 cm^{-1} . 740

Synthesis of $[\text{Fe}^{\text{III}}\text{L1}(\text{OH})](\text{OTf})_2$. Ligand L1 (1.00 g, 2.25 mmol, 741
1.0 equiv) was suspended in 40 mL of water. Iron(III) triflate (1.51 742
mg, 3.00 mmol, 1.3 equiv) was added as a solid. The mixture turned 743
orange-red upon mixing; the mixture was sonicated for 1 h at 40°C 744
which led to a color change to deep red. Additional iron(III) triflate 745
(0.56 g, 1.11 mmol, 0.8 equiv) was added, and the mixture was 746
sonicated briefly. The mixture was filtered through a sintered glass frit, 747
and sodium triflate (775.0 mg, 4.50 mmol) was added as a solid to the 748
filtrate. The mixture was stored at 4°C for 3 days. The formed 749
crystals were washed with water and dried in vacuo to give 750
 $[\text{Fe}^{\text{III}}\text{L1}(\text{OH})](\text{OTf})_2$ (no yield determined). The precipitate 751

752 obtained from filtering was collected and recrystallized from water (40
753 °C) to give $[\text{Fe}^{\text{III}}\text{L1}(\text{OH})](\text{OTf})_2 \times 2 \text{H}_2\text{O}$ (no yield determined).
754 **HR-MS (ESI)**: Calculated for $\text{C}_{29}\text{H}_{26}\text{FeN}_5\text{O}$ $[\text{FeL1}(\text{OH})]^{2+}$:
755 258.07434 *m/z*; Found: 258.07355 *m/z*. **Elemental Analysis**:
756 Calculated for $\text{C}_{31}\text{H}_{26}\text{F}_6\text{FeN}_5\text{O}_7\text{S}_2$: C 45.71, H 3.22, N 8.60, S 7.87.
757 Found: C 44.17, H 3.36, N 8.07, S 7.78. Calculated for
758 $\text{C}_{31}\text{H}_{30}\text{F}_6\text{FeN}_5\text{O}_9\text{S}_2$ ($[\text{Fe}^{\text{III}}\text{L1}(\text{OH})](\text{OTf})_2 \times 2\text{H}_2\text{O}$): C 43.78, H
759 3.56, N 8.23, S 7.54. Found: C 43.53, H 3.42, N 8.06, S 7.99. **IR (thin**
760 **film)**: $\nu \sim$ 3424, 3091, 1657, 1599, 1462, 1447, 1390, 1256, 1224,
761 1154, 1103, 1026, 914, 868, 847, 782, 764, 742, 664 cm^{-1} .

762 **Synthesis of $[\text{Fe}^{\text{IV}}\text{L1}(\text{O})][\text{Ce}(\text{NO}_3)_6]$** . According to a modified
763 literature procedure,^{8,9} $[\text{Fe}^{\text{IV}}\text{L1}(\text{MeCN})](\text{OTf})_2$ (100 mg, 0.119 mmol,
764 1.0 equiv) was dissolved in 1.5 mL of 3:1 acetonitrile:water.
765 Cerium(IV) ammonium nitrate (347.1 mg, 0.633 mmol, 5.3 equiv)
766 was added as a solid, and the mixture was sonicated for 60 s. As a pale
767 green precipitate began to form, the reaction mixture was placed in an
768 ice bath to complete the precipitation. The solid was collected on a
769 sintered glass frit, washed with 1.5 mL of ice cold 3:1 acetonitrile-
770 water, and dried in vacuo to yield product $[\text{Fe}^{\text{IV}}\text{L1}(\text{O})][\text{Ce}(\text{NO}_3)_6]$
771 as a pale green solid (107.2 mg, 87%). **Elemental Analysis**:
772 Calculated for $\text{C}_{29}\text{H}_{25}\text{CeFeN}_{11}\text{O}_{19}$: C 33.90, H 2.45, N 14.99.
773 Found: C 33.81, H 2.58, N 15.20. **ICP-OES**: Fe: 52.3 mg/g $\hat{=}$ 0.937
774 mmol/g; Ce: 131.5 mg/g $\hat{=}$ 0.939 mmol/g; Molecular ratio of Fe:Ce
775 = 1:1. **IR (thin film)**: $\nu \sim$ 1600, 1496, 1277, 1033, 864, 822, 804,
776 784, 760, 742 cm^{-1} . **UV-vis-NIR (H_2O)**: $\lambda = 720 \text{ nm}$ ($\epsilon = 277 \text{ l}$
777 $\text{mol}^{-1} \text{cm}^{-1}$).

778 **Synthesis of Pyridine-2,6-diylbis(pyridin-2-ylmethanone)**
779 **(2)**. According to a modified literature procedure,² a flame-dried
780 flask was charged with 2-bromo pyridine (2.62 mL, 4.25 g, 26.88
781 mmol, 3.0 equiv), and 100 mL of absolute tetrahydrofuran was added.
782 After cooling the mixture to -78°C , a solution of *n*-butyl lithium (2.5
783 M in hexanes, 10.75 mL, 1.72 g, 26.88 mmol, 3.0 equiv) was added
784 dropwise, resulting in a color change to yellowish brown. The mixture
785 was stirred at -78°C for 10 min, and then a solution of 1-(6-(1,1-
786 dipyridin-2-yl)ethyl)pyridin-2-yl)ethan-1-one (0.224 M in tetrahy-
787 drofuran, 40.0 mL, 2.0 g, 8.96 mmol, 1.0 equiv) was added dropwise;
788 the solution's color slowly changed to a very dark green. The reaction
789 was stirred at -78°C for 40 min; then, 50 mL methanol was added
790 slowly to quench the reaction. The mixture was allowed to warm to
791 room temperature, 100 mL of aqueous hydrochloric acid (3 M) was
792 added, and the organic solvents were removed via rotary evaporation
793 (90 mbar at 40°C). The mixture was transferred to a separatory
794 funnel. Additional 10 mL of aqueous hydrochloric acid (3 M) was
795 added, and the mixture was washed with dichloromethane (2×25
796 mL); this organic layer was discarded. The aqueous layer was basified
797 to pH 12 with an aqueous solution of sodium hydroxide (19 M) and
798 extracted with dichloromethane ($3 \times 100 \text{ mL}$). These combined
799 organic layers were dried over anhydrous magnesium sulfate, and the
800 solvents were removed in vacuo to yield the crude product.
801 Recrystallization at room temperature from acetone/diethyl ether
802 gave pure product **2** as a colorless crystalline solid in 67% yield (1.74
803 g). $R_F = 0.13$ (silica, UV, 10% triethyl amine, 50% ethyl acetate, 40%
804 hexanes). **$^1\text{H NMR}$** (400.0 MHz, CDCl_3 , 295 K): $\delta = 8.75$ (ddd, $J =$
805 4.7 Hz, $J = 1.7$ Hz, $J = 0.9$ Hz, 2H), 8.31 (d, $J = 8.0$ Hz, 2H), 8.19 (dt,
806 $J = 7.9$ Hz, $J = 1.1$ Hz, 2H), 8.11 (dd, $J = 8.2$ Hz, $J = 7.4$ Hz, 1H), 7.79
807 (td, $J = 7.8$ Hz, $J = 1.8$ Hz, 2H), 7.45 (ddd, $J = 7.6$ Hz, $J = 4.7$ Hz, $J =$
808 1.2 Hz, 2H) ppm. NMR data are in accordance with the literature.²
809 **HR-MS (ESI)**: Calculated for $\text{C}_{17}\text{H}_{12}\text{N}_3\text{O}_2$ $[\text{M} + \text{H}]^+$: 290.09295 *m/*
810 *z*; Found: 290.09271 *m/z*.

811 **Synthesis of L2**. According to a modified literature procedure,² a
812 flame-dried flask was charged with 2-bromo pyridine (0.36 mL, 0.58 g,
813 3.66 mmol, 2.12 equiv), and 80 mL of absolute tetrahydrofuran was
814 added. After the mixture was cooled to -78°C , a solution of *n*-butyl
815 lithium (2.5 M in hexanes, 1.49 mL, 0.24 g, 3.72 mmol, 2.15 equiv)
816 was added dropwise, resulting in a color change to yellowish brown.
817 The mixture was stirred at -78°C for 10 min, and then a solution of
818 **2** (57.5 mM in tetrahydrofuran/1,4-dioxane (4:1), 30.0 mL, 0.5 g,
819 1.73 mmol, 1.0 equiv) was added dropwise, and the solution's color
820 changed first to red and then to a very dark green. The reaction was
821 stirred at -78°C for 60 min, then allowed to warm to room

temperature. When LC-MS confirmed complete consumption of **2**, 822
50 mL of methanol was added slowly to quench the reaction. Then, 823
100 mL of aqueous hydrochloric acid (3 M) was added, the organic 824
solvents were removed via rotary evaporation (90 mbar @ 40°C), 825
and the mixture was transferred to a separatory funnel. An additional 826
10 mL of aqueous hydrochloric acid (3 M) was added, and the 827
mixture was washed with dichloromethane ($2 \times 25 \text{ mL}$); this organic 828
layer was discarded. The aqueous layer was basified to pH 12 with an 829
aqueous solution of sodium hydroxide (19 M) and extracted with 830
dichloromethane ($3 \times 100 \text{ mL}$). These combined organic layers were 831
dried over anhydrous magnesium sulfate, and the solvents were 832
removed in vacuo to yield the crude product. Recrystallization at 833
room temperature from acetone/diethyl ether gave the pure product 834
L2 as a colorless solid in a 38% yield (290.0 mg). $R_F = 0.04$ (silica, 835
UV, 10% methanol, 90% dichloromethane) **$^1\text{H NMR}$** (400.0 MHz, 836
 CDCl_3 , 295 K): $\delta = 8.49$ (ddd, $J = 4.9$ Hz, $J = 1.8$ Hz, $J = 1.0$ Hz, 4H), 837
7.73–7.71 (m, 3H), 7.52 (ddd, $J = 8.0$ Hz, $J = 7.3$ Hz, $J = 1.8$ Hz, 838
4H), 7.44 (dt, $J = 8.0$ Hz, $J = 1.1$ Hz, 4H), 7.17–7.13 (m, 6H) ppm. 839
NMR data are in accordance with the literature.² **HR-MS (ESI)**: 840
Calculated for $\text{C}_{27}\text{H}_{22}\text{N}_5\text{O}_2$ $[\text{M} + \text{H}]^+$: 448.17735 *m/z*; Found: 841
448.17693 *m/z*. 842

Synthesis of $[\text{Fe}^{\text{II}}\text{L2}(\text{MeCN})](\text{OTf})_2$. According to a modified 843
literature procedure,^{8,9} ligand **L2** (51.0 mg, 0.114 mmol, 1.0 equiv) 844
was dissolved in 2.55 mL of acetonitrile. Iron(II)bis(acetonitrile)bis- 845
(triflate) (49.7 mg, 0.114 mmol, 1.0 equiv) was added as a solid, 846
turning the solution deep red. The mixture was then stirred for an 847
additional 5 min, and then diethyl ether was diffused into the solution 848
under ambient conditions to give the product $[\text{Fe}^{\text{II}}\text{L2}(\text{MeCN})]-$ 849
 $(\text{OTf})_2 \times \text{H}_2\text{O}$ as brown crystals in 77% yield (80.0 mg). **$^1\text{H NMR}$** 850
(400.0 MHz, CD_3CN , 295 K): $\delta = 9.73$ (d, $J = 5.8$ Hz, 4H, H_{py}), 8.17 851
(m, 5H, $\text{H}_{\text{py}}/\text{H}-2/\text{H}-3$), 7.98 (ddd, $J = 8.1$ Hz, $J = 7.4$ Hz, $J = 1.4$ Hz, 852
4H, H_{py}), 7.56 (ddd, $J = 7.4$ Hz, $J = 5.8$ Hz, $J = 1.5$ Hz, 4H, H_{py}), 6.85 853
(s, 2H, OH), 1.96 (s, 3H, CH_3CN) ppm. **$^{13}\text{C NMR}$** (100.0 MHz, 854
 CD_3CN , 295 K): $\delta = 164.5$ ($\text{C}_{\text{py-quat}}$), 163.1 (C-1), 158.1 (C_{py}), 855
140.7 (C-2), 140.0 (C_{py}), 124.9 (C_{py}), 122.4 (C_{py}), 121.0 (C-3), 80.7 856
(C-4) ppm. **HR-MS (ESI)**: Calculated for $\text{C}_{30}\text{H}_{25}\text{F}_6\text{FeN}_5\text{O}_3\text{S}$ 857
 $[\text{FeL2}(\text{OTf})]^{+}$: 652.05649 *m/z*; Found: 652.05432 *m/z*. **Elemental** 858
Analysis: Calculated for $\text{C}_{33}\text{H}_{30}\text{F}_6\text{FeN}_6\text{O}_7\text{S}_2$ ($[\text{Fe}^{\text{II}}\text{L2}(\text{MeCN})]-$ 859
 $(\text{OTf})_2 \times \text{H}_2\text{O}$): C 43.27, H 3.05, N 9.77, S 7.45. Found: C 43.25, 860
H 3.12, N 9.79, S 7.91. **IR (thin film)**: $\nu \sim$ 3288, 1738, 1603, 1469, 861
1444, 1373, 1276, 1244, 1224, 1157, 1096, 1028, 887, 800, 762, 712, 862
661 cm^{-1} . **UV-vis-NIR (MeCN)**: $\lambda = 347 \text{ nm}$ ($\epsilon = 5315 \text{ l mol}^{-1}$ 863
 cm^{-1}); $\lambda = 420 \text{ nm}$ ($\epsilon = 5415 \text{ l mol}^{-1} \text{cm}^{-1}$). 864

Synthesis of $[\text{Fe}^{\text{III}}\text{L2}(\text{OH})](\text{OTf})_2$. A scintillation vial was charged 865
with finely ground **L2** (200.0 mg, 0.447 mmol, 1.0 equiv) and 1.1 mL 866
of water. Iron(III) triflate (247.3 mg, 0.492 mmol, 1.1 equiv) was 867
added, and the suspension was mixed by pumping of an Eppendorf 868
pipet. The mixture was sonicated for 60 s, shaken, and again sonicated 869
for 60 s, resulting in a dark red suspension. The mixture was then 870
syringe-filtered (PTFE, 0.45 μm) to give a clear red-orange solution. 871
This was placed in a fridge at 4°C for 3 days until dark red crystals 872
had formed. The supernatant was removed, and the crystals were 873
washed with water ($2 \times 0.5 \text{ mL}$, brief sonication) and subsequently 874
dried in vacuo to give the pure product $[\text{Fe}^{\text{III}}\text{L2}(\text{OH})](\text{OTf})_2$ as 875
brown crystals (67%). **HR-MS (EI)**: Calculated for $\text{C}_{27}\text{H}_{22}\text{FeN}_5\text{O}_3$ 876
 $[\text{FeL2}(\text{OH})]^{2+}$: 260.0536 *m/z*; Found: 260.0548 *m/z*. **Elemental** 877
Analysis: Calculated for $\text{C}_{29}\text{H}_{24}\text{F}_6\text{FeN}_5\text{O}_{10}\text{S}_2$ ($[\text{FeL2}(\text{OH})](\text{OTf})_2 \times$ 878
 H_2O): C 41.64, H 2.89, N 8.37, S 7.67. Found: C 41.71, H 2.92, N 879
8.24, S 7.94. **IR (thin film)**: $\nu \sim$ 3450, 3264, 1739, 1604, 1458, 880
1445, 1364, 1278, 1243, 1222, 1152, 1097, 1027, 927, 810, 795, 766, 881
741, 675, 662 cm^{-1} . 882

Synthesis of $[\text{Fe}^{\text{IV}}\text{L2}(\text{O})][\text{Ce}(\text{NO}_3)_6]$. According to a modified 883
literature procedure,^{8,9} $[\text{Fe}^{\text{IV}}\text{L2}(\text{MeCN})](\text{OTf})_2$ (80 mg, 0.950 mmol, 884
1.0 equiv) was dissolved in 1.2 mL of 3:1 acetonitrile:water. 885
Cerium(IV) ammonium nitrate (276.4 mg, 0.504 mmol, 5.3 equiv) 886
was added as a solid, and the mixture was sonicated for 60 s. As a pale 887
green precipitate began to form, the reaction mixture was placed in 888
the refrigerator at 4°C to complete the precipitation. The solid was 889
collected via centrifugation (600 rpm), washed with 10.5 mL of ice 890
cold 3:1 acetonitrile:water, and dried in vacuo to yield product 891

892 $[\text{Fe}^{\text{IV}}\text{L2}(\text{O})][\text{Ce}(\text{NO}_3)_6]$ as a pale green solid (89%). **Elemental**
893 **Analysis:** Calculated for $\text{C}_{27}\text{H}_{23}\text{CeFeN}_{11}\text{O}_{22}$ ($[\text{Fe}^{\text{IV}}\text{L2}(\text{O})][\text{Ce}$
894 $(\text{NO}_3)_6] \times \text{H}_2\text{O}$): C 30.90, H 2.21, N 14.68. Found: C 30.71, H
895 2.54, N 15.05. **HR-MS** (ESI): Calculated for $\text{C}_{27}\text{H}_{21}\text{FeN}_9\text{O}_3$
896 $[\text{Fe}^{\text{IV}}\text{L2}(\text{O})]^{2+}$: 259.5497 *m/z*; Found: 259.5492 *m/z*. **IR** (**thin**
897 **film**): ν = 1605, 1504, 1463, 1278, 1170, 1098, 1029, 830, 805, 780,
898 763, 742, 661, 626, 614 cm^{-1} . **UV-vis-NIR** (H_2O): λ = 720 nm (ϵ =
899 292 $\text{L mol}^{-1} \text{cm}^{-1}$).

900 **Reaction Rate Determination via UV-Vis-NIR Spectroscopy.** Benzyl alcohol, benzaldehyde, and ethylbenzenesulfonic acid were
901 used as substrates. An aqueous solution of $[\text{Fe}^{\text{IV}}\text{L1}(\text{O})]^{2+}$ or
902 $[\text{Fe}^{\text{IV}}\text{L2}(\text{O})]^{2+}$ (25 μL , 10 mM, 1 equiv) was diluted with water
903 (450 μL), and this mixture was added to a 500 μL cuvette with an
904 aqueous solution of the substrate (25 μL , 10 mM, 1 equiv).
905 Measurements were started immediately after addition, and spectra
906 were recorded over a time period of 15 min. The method of initial
907 rates was applied to calculate the reaction rate constants. The
908 obtained absorption values were converted to concentrations using
909 the Lambert-Beer Law. The therefore needed extinction coefficient
910 was obtained by recording UV-vis-NIR spectra of the complexes in
911 different concentrations and applying linear regression on a plot of
912 absorbance against concentration (ϵ = 277.2 $\text{L mol}^{-1} \text{cm}^{-1}$ for
913 $[\text{Fe}^{\text{IV}}\text{L1}(\text{O})]^{2+}$ and ϵ = 291.6 $\text{L mol}^{-1} \text{cm}^{-1}$ for $[\text{Fe}^{\text{IV}}\text{L2}(\text{O})]^{2+}$).
914 Reaction rates were obtained by linear regression of the decreasing
915 concentrations and transformed into rate constants. For results, refer
916 to Table S2, p 7.

917 **Product Identification via ^1H NMR Spectroscopy-BnOH**
918 **and PhCHO.** All aqueous solutions were prepared in deuterated
919 water. Benzyl alcohol and benzaldehyde were used as substrates. A
920 solution of the substrate in deuterated water (400 μL , 10 mM, 1
921 equiv) was mixed with a solution of $[\text{Fe}^{\text{IV}}\text{L1}(\text{O})]^{2+}$ or $[\text{Fe}^{\text{IV}}\text{L2}(\text{O})]^{2+}$
922 in deuterated water (400 μL , 10 mM, 1 equiv) and reacted for 30 min
923 at 25 °C. A solution of deuterated hydrochloric acid in deuterated
924 water (400 μL , 2 mM) was added, and the reaction solution was
925 extracted with deuterated chloroform ($2 \times 400 \mu\text{L}$). The combined
926 organic phases were transferred into an NMR tube, and a ^1H NMR
927 spectrum was recorded.

928 **Product Identification via ^1H NMR Spectroscopy-EBS.** A
929 solution of ethylbenzenesulfonic acid (EBS) in deuterated water (500
930 μL , 10 mM, 1 equiv) was mixed with a solution of $[\text{Fe}^{\text{IV}}\text{L1}(\text{O})]^{2+}$ or
931 $[\text{Fe}^{\text{IV}}\text{L2}(\text{O})]^{2+}$ in deuterated water (500 μL , 10 mM, 1 equiv) and
932 reacted for 30 min at 25 °C. The reaction mixture was filtered over
933 silica (1 mL syringe equipped with cotton and silica filled to the 0.5
934 mL mark). The colorless filtrate was transferred into an NMR tube,
935 and a ^1H NMR spectrum recorded.

937 ■ ASSOCIATED CONTENT

938 ■ Supporting Information

939 The Supporting Information is available free of charge at
940 <https://pubs.acs.org/doi/10.1021/acs.inorgchem.4c04518>.

941 General methods and materials, synthetic procedures,
942 additional ^1H and ^{13}C NMR spectra, UV-vis-NIR
943 spectra, cyclic voltammograms, stopped-flow UV-vis
944 data (CSV), cryo UHR-MS spectra, LC-MS data,
945 Mössbauer spectra, crystallographic information, and
946 EPR spectra (TXT, DSC, and DTA) (PDF)

947 Accession Codes

948 Deposition Numbers 2314071–2314072 and 2320855 contain
949 the supplementary crystallographic data for this paper. These
950 data can be obtained free of charge via the joint Cambridge
951 Crystallographic Data Centre (CCDC) and Fachinformations-
952 zentrum Karlsruhe Access Structures service.

953 ■ AUTHOR INFORMATION

954 Corresponding Author

955 Lena J. Daumann – Department of Chemistry, Ludwig-
956 Maximilians-University Munich, 81377 München, Germany;

Mathematisch Naturwissenschaftliche Fakultät, Lehrstuhl für
957 Bioanorganische Chemie, Heinrich-Heine-Universität, 40225
958 Düsseldorf, Germany; orcid.org/0000-0003-2197-136X;
959 Email: lena.daumann@hhu.de
960

961 Authors

Niko S. W. Lindlar né Jonasson – Department of Chemistry,
962 Ludwig-Maximilians-University Munich, 81377 München,
963 Germany; Department of Chemistry, University of Zurich,
964 8057 Zurich, Switzerland; orcid.org/0000-0002-6034-6164
965

Annika Menke – Department of Chemistry, Ludwig-
966 Maximilians-University Munich, 81377 München, Germany
967

Laura Senft – Department of Chemistry, Ludwig-Maximilians-
968 University Munich, 81377 München, Germany
969

Andrea Squarcina – Department of Chemistry, Ludwig-
970 Maximilians-University Munich, 81377 München, Germany;
971 orcid.org/0000-0003-1770-586X
972

David Schmidl – Department of Chemistry, Ludwig-
973 Maximilians-University Munich, 81377 München, Germany;
974 Department of Chemical and Pharmaceutical Sciences,
975 London Metropolitan University, London N7 8DB, U.K.;
976 Present Address: Department of Chemistry, University of
977 Cambridge, Lensfield Road, Cambridge CB2 1EW, U.K.
978

Katherine Fisher – Department of Chemistry, Ludwig-
979 Maximilians-University Munich, 81377 München, Germany;
980 Department of Chemical and Pharmaceutical Sciences,
981 London Metropolitan University, London N7 8DB, U.K.;
982 orcid.org/0000-0002-2716-561X
983

Serhiy Demeshko – Institute of Inorganic Chemistry, Georg-
984 August-Universität Göttingen, 37077 Göttingen, Germany
985

Jan C. Kruse – Institute of Inorganic Chemistry, Georg-
986 August-Universität Göttingen, 37077 Göttingen, Germany;
987 orcid.org/0009-0003-5564-8090
988

Thomas Josephy – Institute of Inorganic Chemistry, Ruprecht-
989 Karls-Universität Heidelberg, 69120 Heidelberg, Germany
990

Peter Mayer – Department of Chemistry, Ludwig-
991 Maximilians-University Munich, 81377 München, Germany
992

Jonathan Gutenthaler-Tietze – Department of Chemistry,
993 Ludwig-Maximilians-University Munich, 81377 München,
994 Germany
995

Peter Comba – Institute of Inorganic Chemistry, Ruprecht-
996 Karls-Universität Heidelberg, 69120 Heidelberg, Germany;
997 orcid.org/0000-0001-7796-3532
998

Franc Meyer – Institute of Inorganic Chemistry, Georg-
999 August-Universität Göttingen, 37077 Göttingen, Germany;
1000 orcid.org/0000-0002-8613-7862
1001

Ivana Ivanović-Burmazović – Department of Chemistry,
1002 Ludwig-Maximilians-University Munich, 81377 München,
1003 Germany
1004

Complete contact information is available at:
1005 <https://pubs.acs.org/10.1021/acs.inorgchem.4c04518>
1006

1007 Author Contributions

The manuscript was written through contributions of all
1008 authors. All authors have given approval to the final version of
1009 the manuscript. N.S.W.L. and A.M. developed the project,
1010 accomplished the synthetic work, performed the UV-vis-NIR
1011 experiments, and wrote the manuscript. L.S. carried out the
1012 UHR-MS measurements as well as simulations thereof,
1013 supervised by I.I.-B. A.S. performed cyclic voltammetry
1014 investigations and interpretations, supervised by I.I.-B. D.S.
1015 was involved in the discovery of the comproportionation
1016

1018 reaction and contributed in the synthesis and crystallization of
1019 $[\text{Fe}^{\text{III}}\text{LI}(\text{OH})]^{2+}$. K.F. simulated the EPR spectra. SD and
1020 J.C.K. performed the Mössbauer measurements and J.C.K.
1021 accomplished cyclic voltammetry investigations and interpre-
1022 tation concerning the pourbaix diagram, supervised by F.M.,
1023 T.J. carried out stopped-flow UV-vis-NIR measurements,
1024 supervised by P.C., P.M. and J. G.-T. performed the X-ray
1025 measurements and solution of the crystal structures. L.J.D.
1026 coordinated and supervised the whole project. N.S.W.L. and
1027 A.M. contributed equally to this work.

1028 Funding

1029 This work was funded by the Deutsche Forschungsgemein-
1030 schaft (DFG, German Research Foundation)–SFB 1309-
1031 325871075 and FOR 5215 in the framework of the Research
1032 Unit “Bioinspired Oxidation Catalysis with Iron Complexes”
1033 (BioOxCat). N.S.W.L. thankfully acknowledges support by the
1034 Studienstiftung des deutschen Volkes and the Joachim-Herz-
1035 Foundation. J.C.K. acknowledges support by the Fonds der
1036 Chemischen Industrie (Kekulé fellowship).

1037 Notes

1038 The authors declare no competing financial interest.

1039 ■ ACKNOWLEDGMENTS

1040 A.M. thanks Jan Prohaska and Sophie Falkai for their work in
1041 this project. N.S.W.L. wishes to thank Katharina Scholz and
1042 Hannah Wilken for their help in this project.

1043 ■ REFERENCES

1044 (1) Goldsmith, C. R.; Jonas, R. T.; Stack, T. D. P. C-H bond
1045 activation by a ferric methoxide complex: modeling the rate-
1046 determining step in the mechanism of lipoxygenase. *J. Am. Chem.*
1047 *Soc.* **2002**, *124* (1), 83–96.
1048 (2) Goldsmith, C. R.; Stack, T. D. P. Hydrogen atom abstraction by
1049 a mononuclear ferric hydroxide complex: insights into the reactivity of
1050 lipoxygenase. *Inorg. Chem.* **2006**, *45* (15), 6048–6055.
1051 (3) Das, B.; Orthaber, A.; Ott, S.; Thapper, A. Iron Pentapyridyl
1052 Complexes as Molecular Water Oxidation Catalysts: Strong Influence
1053 of a Chloride Ligand and pH in Altering the Mechanism.
1054 *ChemSusChem* **2016**, *9* (10), 1178–1186.
1055 (4) Gupta, R.; Borovik, A. S. Monomeric Mn III/II and Fe III/II
1056 Complexes with Terminal Hydroxo and Oxo Ligands: Probing
1057 Reactivity via O–H Bond Dissociation Energies. *J. Am. Chem. Soc.*
1058 **2003**, *125* (43), 13234–13242.
1059 (5) Mukherjee, J.; Lucas, R. L.; Zart, M. K.; Powell, D. R.; Day, V.
1060 W.; Borovik, A. S. Synthesis, structure, and physical properties for a
1061 series of monomeric iron(III) hydroxo complexes with varying
1062 hydrogen-bond networks. *Inorg. Chem.* **2008**, *47* (13), 5780–5786.
1063 (6) Drummond, M. J.; Ford, C. L.; Gray, D. L.; Popescu, C. V.;
1064 Fout, A. R. Radical Rebound Hydroxylation Versus H-Atom Transfer
1065 in Non-Heme Iron(III)-Hydroxo Complexes: Reactivity and Struc-
1066 tural Differentiation. *J. Am. Chem. Soc.* **2019**, *141* (16), 6639–6650.
1067 (7) Ching, W.-M.; Zhou, A.; Klein, J. E. M. N.; Fan, R.; Knizia, G.;
1068 Cramer, C. J.; Guo, Y.; Que, L. Characterization of the Fleeting
1069 Hydroxoiron(III) Complex of the Pentadentate TMC-py Ligand.
1070 *Inorg. Chem.* **2017**, *56* (18), 11129–11140.
1071 (8) Chantarojsiri, T.; Sun, Y.; Long, J. R.; Chang, C. J. Water-
1072 Soluble Iron(IV)-Oxo Complexes Supported by Pentapyridine
1073 Ligands: Axial Ligand Effects on Hydrogen Atom and Oxygen
1074 Atom Transfer Reactivity. *Inorg. Chem.* **2015**, *54* (12), 5879–5887.
1075 (9) Jonasson, N. S. W.; Daumann, L. J. 5-Methylcytosine is Oxidized
1076 to the Natural Metabolites of TET Enzymes by a Biomimetic
1077 Iron(IV)-Oxo Complex. *Chem.—Eur. J.* **2019**, *25* (52), 12091–
1078 12097.
1079 (10) Schmidl, D.; Jonasson, N. S. W.; Korytiaková, E.; Carell, T.;
1080 Daumann, L. J. Biomimetic Iron Complex Achieves TET Enzyme
1081 Reactivity*. *Angew. Chem., Int. Ed.* **2021**, *60* (39), 21457–21463.

(11) Jonasson, N. S. W.; Janßen, R.; Menke, A.; Zott, F. L.; Zipse, 1082
H.; Daumann, L. J. TET-Like Oxidation in 5-Methylcytosine and 1083
Derivatives: A Computational and Experimental Study. *ChemBio-* 1084
Chem. **2021**, *22* (23), 3333–3340.

(12) Puri, M.; Que, L. Toward the synthesis of more reactive S = 2 1086
non-heme oxoiron(IV) complexes. *Acc. Chem. Res.* **2015**, *48* (8), 1087
2443–2452.

(13) Rasheed, W.; Fan, R.; Abelson, C. S.; Peterson, P. O.; Ching, 1089
W.-M.; Guo, Y.; Que, L. Structural implications of the paramagneti- 1090
cally shifted NMR signals from pyridine H atoms on synthetic 1091
nonheme FeIV = O complexes. *J. Biol. Inorg. Chem.* **2019**, *24* (4), 1092
533–545.

(14) Abu-Odeh, M.; Bleher, K.; Johnee Britto, N.; Comba, P.; Gast, 1094
M.; Jaccob, M.; Kersch, M.; Krieg, S.; Kurth, M. Pathways of the 1095
Extremely Reactive Iron(IV)-oxido complexes with Tetradentate 1096
Bispidine Ligands. *Chemistry—A European Journal* **2021**, *27* (44), 1097
11377–11390.

(15) Pistorius, E. K.; Axelrod, B. Iron, an Essential Component of 1099
Lipoxygenase. *J. Biol. Chem.* **1974**, *249* (10), 3183–3186.

(16) *Active Oxygen in Biochemistry*; Valentine, J. S.; Foote, C. S.; 1101
Greenberg, A.; Liebman, J. F., Eds.; Springer US, 1995.

(17) Andreou, A.; Feussner, I. Lipoxygenases - Structure and 1103
reaction mechanism. *Phytochemistry* **2009**, *70* (13–14), 1504–1510.

(18) Gaffney, B. J. EPR Spectroscopic Studies of Lipoxygenases. 1105
Chem.—Asian J. **2020**, *15* (1), 42–50.

(19) Schilstra, M. J.; Veldink, G. A.; Vliegthart, J. F. The 1107
dioxygenation rate in lipoxygenase catalysis is determined by the 1108
amount of iron (III) lipoxygenase in solution. *Biochem.* **1994**, *33* (13), 1109
3974–3979.

(20) Price, J. C.; Barr, E. W.; Glass, T. E.; Krebs, C.; Bollinger, J. M. 1111
Evidence for hydrogen abstraction from C1 of taurine by the high- 1112
spin Fe(IV) intermediate detected during oxygen activation by 1113
taurine:alpha-ketoglutarate dioxygenase (TauD). *J. Am. Chem. Soc.* 1114
2003, *125* (43), 13008–13009.

(21) Price, J. C.; Barr, E. W.; Tirupati, B.; Bollinger, J. M.; Krebs, C. 1116
The first direct characterization of a high-valent iron intermediate in 1117
the reaction of an alpha-ketoglutarate-dependent dioxygenase: a high- 1118
spin FeIV complex in taurine/alpha-ketoglutarate dioxygenase 1119
(TauD) from *Escherichia coli*. *Biochemistry* **2003**, *42* (24), 7497– 1120
7508.

(22) Proshlyakov, D. A.; Henshaw, T. F.; Monterosso, G. R.; Ryle, 1122
M. J.; Hausinger, R. P. Direct detection of oxygen intermediates in the 1123
non-heme Fe enzyme taurine/alpha-ketoglutarate dioxygenase. *J. Am.* 1124
Chem. Soc. **2004**, *126* (4), 1022–1023.

(23) Price, J. C.; Barr, E. W.; Hoffart, L. M.; Krebs, C.; Bollinger, J. 1126
M. Kinetic dissection of the catalytic mechanism of taurine:alpha- 1127
ketoglutarate dioxygenase (TauD) from *Escherichia coli*. *Biochem.* 1128
2005, *44* (22), 8138–8147.

(24) Matsui, K. Green leaf volatiles: hydroperoxide lyase pathway of 1130
oxylipin metabolism. *Curr. Opin. Plant Biol.* **2006**, *9* (3), 274–280.

(25) Jasniewski, A. J.; Que, L. Dioxygen Activation by Nonheme 1132
Diiron Enzymes: Diverse Dioxygen Adducts, High-Valent Intermedi- 1133
ates, and Related Model Complexes. *Chem. Rev.* **2018**, *118* (5), 1134
2554–2592.

(26) Krebs, C.; Price, J. C.; Baldwin, J.; Saleh, L.; Green, M. T.; 1136
Bollinger, J. M. Rapid freeze-quench 57Fe Mössbauer spectroscopy: 1137
monitoring changes of an iron-containing active site during a 1138
biochemical reaction. *Inorg. Chem.* **2005**, *44* (4), 742–757.

(27) Islam, M. S.; Leissing, T. M.; Chowdhury, R.; Hopkinson, R. J.; 1140
Schofield, C. J. 2-Oxoglutarate-Dependent Oxygenases. *Annu. Rev.* 1141
Biochem. **2018**, *87*, 585–620.

(28) Tagliapietra, M.; Squarcina, A.; Hickey, N.; De Zorzi, R.; 1143
Geremia, S.; Sartorel, A.; Bonchio, M. Hydrogen Evolution by FeIII 1144
Molecular Electrocatalysts Interconverting between Mono and Di- 1145
Nuclear Structures in Aqueous Phase. *ChemSusChem* **2017**, *10* (22), 1146
4430–4435.

(29) Ghosh, S. K.; Rath, S. P. A remarkably bent diiron(III)-μ- 1148
hydroxo bisporphyrin: unusual stabilization of two spin states of iron 1149

- 1150 in a single molecular framework. *J. Am. Chem. Soc.* **2010**, *132* (51), 1151 17983–17985.
- 1152 (30) Tanase, S.; Bouwman, E.; Long, G. J.; Shahin, A. M.; Mills, A. 1153 M.; Spek, A. L.; Reedijk, J. Acid-Base Self-Assembly Chemistry and 1154 Hydrogen Bonding Interactions Resulting in the Formation of a 1155 Tetranuclear Aggregate Containing Four Crystallographically Non- 1156 Equivalent Fe III Centers. *Eur. J. Inorg. Chem.* **2004**, *2004* (23), 1157 4572–4578.
- 1158 (31) Cordes Née Kupper, C.; Morganti, M.; Klawitter, I.; 1159 Schremmer, C.; Dechert, S.; Meyer, F. Disproportionation Equili- 1160 brium of a μ -Oxodiiron(III) Complex Giving Rise to C-H Activation 1161 Reactivity: Structural Snapshot of a Unique Oxoiron(IV) Adduct. 1162 *Angew. Chem., Int. Ed.* **2019**, *58* (32), 10855–10858.
- 1163 (32) Minor, W.; Steczko, J.; Stec, B.; Otwinowski, Z.; Bolin, J. T.; 1164 Walter, R.; Axelrod, B. Crystal structure of soybean lipoxygenase L-1 1165 at 1.4 Å resolution. *Biochem.* **1996**, *35* (33), 10687–10701.
- 1166 (33) Cho, K.-B.; Wu, X.; Lee, Y.-M.; Kwon, Y. H.; Shaik, S.; Nam, 1167 W. Evidence for an alternative to the oxygen rebound mechanism in 1168 C-H bond activation by non-heme Fe(IV)O complexes. *J. Am. Chem.* 1169 *Soc.* **2012**, *134* (50), 20222–20225.
- 1170 (34) Horn, A.; Vencato, I.; Bortoluzzi, A. J.; Hörner, R.; Silva, R. A. 1171 N.; Spoganicz, B.; Drago, V.; Terenzi, H.; de Oliveira, M. C. B.; 1172 Werner, R.; Haase, W.; Neves, A. Synthesis, crystal structure and 1173 properties of dinuclear iron(III) complexes containing terminally 1174 coordinated phenolate/H₂O/OH–groups as models for purple acid 1175 phosphatases: efficient hydrolytic DNA cleavage. *Inorg. Chim. Acta* 1176 **2005**, *358* (2), 339–351.
- 1177 (35) Bernhardt, P. V.; Bosch, S.; Comba, P.; Gahan, L. R.; Hanson, 1178 G. R.; Mereacre, V.; Noble, C. J.; Powell, A. K.; Schenk, G.; 1179 Wadepohl, H. An Approach to More Accurate Model Systems for 1180 Purple Acid Phosphatases (PAPs). *Inorg. Chem.* **2015**, *54* (15), 7249– 1181 7263.
- 1182 (36) Zimmermann, T. P.; Limpke, T.; Orth, N.; Franke, A.; 1183 Stammmer, A.; Bögge, H.; Walleck, S.; Ivanovic-Burmazovic, I.; Glaser, 1184 T. Two Unsupported Terminal Hydroxido Ligands in a μ -Oxo- 1185 Bridged Ferric Dimer: Protonation and Kinetic Lability Studies. *Inorg.* 1186 *Chem.* **2018**, *57* (16), 10457–10468.
- 1187 (37) Kripli, B.; Sólyom, B.; Speier, G.; Kaizer, J. Stability and 1188 Catalase-Like Activity of a Mononuclear Non-Heme Oxoiron(IV) 1189 Complex in Aqueous Solution. *Molecules* **2019**, *24* (18), 3236.
- 1190 (38) Yeh, C.-C. G.; Hörner, G.; de Visser, S. P. Computational 1191 Study on O–O Bond Formation on a Mononuclear Non-Heme Iron 1192 Center. *Eur. J. Inorg. Chem.* **2020**, *2020* (27), 2573–2581.
- 1193 (39) Rohde, J.; In, J.; Lim, M. H.; Brennessel, W. W.; Bukowski, M. 1194 R.; Stubna, A.; Münck, E.; Nam, W.; Que, L. Crystallographic and 1195 Spectroscopic Characterization of a Nonheme Fe(IV)=O Complex. 1196 *Science* **2003**, *299*, 1037–1039.
- 1197 (40) Yadav, V.; Gordon, J. B.; Siegler, M. A.; Goldberg, D. P. 1198 Dioxygen-Derived Nonheme Mononuclear FeIII(OH) Complex and 1199 Its Reactivity with Carbon Radicals. *J. Am. Chem. Soc.* **2019**, *141* (26), 1200 10148–10153.
- 1201 (41) Ogo, S.; Wada, S.; Watanabe, Y.; Iwase, M.; Wada, A.; Harata, 1202 M.; Jitsukawa, K.; Masuda, H.; Einaga, H. Synthesis, Structure, and 1203 Spectroscopic Properties of [Feiii(tnpa)(OH)(PhCOO)]ClO₄: A 1204 Model Complex for an Active Form of Soybean Lipoxygenase-1. 1205 *Angew. Chem., Int. Ed.* **1998**, *37* (15), 2102–2104.
- 1206 (42) Ogo, S.; Yamahara, R.; Roach, M.; Suenobu, T.; Aki, M.; 1207 Ogura, T.; Kitagawa, T.; Masuda, H.; Fukuzumi, S.; Watanabe, Y. 1208 Structural and spectroscopic features of a cis (hydroxo)-Fe(III)- 1209 (carboxylato) configuration as an active site model for lipoxygenases. 1210 *Inorg. Chem.* **2002**, *41* (21), 5513–5520.
- 1211 (43) Sahu, S.; Quesne, M. G.; Davies, C. G.; Dürr, M.; Ivanović- 1212 Burmazović, I.; Siegler, M. A.; Jameson, G. N. L.; de Visser, S. P.; 1213 Goldberg, D. P. Direct observation of a nonheme iron(IV)-oxo 1214 complex that mediates aromatic C-F hydroxylation. *J. Am. Chem. Soc.* 1215 **2014**, *136* (39), 13542–13545.
- 1216 (44) England, J.; Martinho, M.; Farquhar, E. R.; Frisch, J. R.; 1217 Bominaar, E. L.; Münck, E.; Que, L. A synthetic high-spin 1218 oxoiron(IV) complex: generation, spectroscopic characterization, 1219 and reactivity. *Angew. Chem., Int. Ed.* **2009**, *48* (20), 3622–3626.
- (45) England, J.; Guo, Y.; van Heuvelen, K. M.; Cranswick, M. A.; 1220 Rohde, G. T.; Bominaar, E. L.; Münck, E.; Que, L. A more reactive 1221 trigonal-bipyramidal high-spin oxoiron(IV) complex with a cis-labile 1222 site. *J. Am. Chem. Soc.* **2011**, *133* (31), 11880–11883. 1223
- (46) Gupta, R.; Lacy, D. C.; Bominaar, E. L.; Borovik, A. S.; 1224 Hendrich, M. P. Electron paramagnetic resonance and Mössbauer 1225 spectroscopy and density functional theory analysis of a high-spin 1226 Fe(IV)-oxo complex. *J. Am. Chem. Soc.* **2012**, *134* (23), 9775–9784. 1227
- (47) Boniolo, M.; Hossain, M. K.; Chernev, P.; Suremann, N. F.; 1228 Heizmann, P. A.; Lyvik, A. S. L.; Beyer, P.; Haumann, M.; Huang, P.; 1229 Salhi, N.; Cheah, M. H.; Shylin, S. I.; Lundberg, M.; Thapper, A.; 1230 Messinger, J. Water Oxidation by Pentapyridyl Base Metal 1231 Complexes? A Case Study. *Inorg. Chem.* **2022**, *61* (24), 9104–9118. 1232
- (48) Boniolo, M.; Chernev, P.; Cheah, M. H.; Heizmann, P. A.; 1233 Huang, P.; Shylin, S. I.; Salhi, N.; Hossain, M. K.; Gupta, A. K.; 1234 Messinger, J.; Thapper, A.; Lundberg, M. Electronic and geometric 1235 structure effects on one-electron oxidation of first-row transition 1236 metals in the same ligand framework. *Dalton Trans.* **2021**, *50* (2), 1237 660–674. 1238
- (49) Elgrishi, N.; Rountree, K. J.; McCarthy, B. D.; Rountree, E. S.; 1239 Eisenhart, T. T.; Dempsey, J. L. A Practical Beginner's Guide to 1240 Cyclic Voltammetry. *J. Chem. Educ.* **2018**, *95* (2), 197–206. 1241
- (50) Jonas, R. T.; Stack, T. D. P. C–H Bond Activation by a Ferric 1242 Methoxide Complex: A Model for the Rate-Determining Step in the 1243 Mechanism of Lipoxygenase. *J. Am. Chem. Soc.* **1997**, *119* (36), 1244 8566–8567. 1245
- (51) Hu, L.; Lu, J.; Cheng, J.; Rao, Q.; Li, Z.; Hou, H.; Lou, Z.; 1246 Zhang, L.; Li, W.; Gong, W.; Liu, M.; Sun, C.; Yin, X.; Li, J.; Tan, X.; 1247 Wang, P.; Wang, Y.; Fang, D.; Cui, Q.; Yang, P.; He, C.; Jiang, H.; 1248 Luo, C.; Xu, Y. Structural insight into substrate preference for TET- 1249 mediated oxidation. *Nature* **2015**, *527* (7576), 118–122. 1250
- (52) Hanauke-Abel, H. M.; Günzler, V. A stereochemical concept 1251 for the catalytic mechanism of prolylhydroxylase: applicability to 1252 classification and design of inhibitors. *J. Theor. Biol.* **1982**, *94* (2), 1253 421–455. 1254
- (53) Rana, S.; Dey, A.; Maiti, D. Mechanistic elucidation of C-H 1255 oxidation by electron rich non-heme iron(IV)-oxo at room temper- 1256 ature. *Chem. Commun.* **2015**, *51* (77), 14469–14472. 1257
- (54) Xie, J.; Lo, P.-K.; Lam, C.-S.; Lau, K.-C.; Lau, T.-C. A 1258 hydrogen-atom transfer mechanism in the oxidation of alcohols by 1259 FeO₄²⁻ in aqueous solution. *Dalton Trans.* **2018**, *47* (1), 240–245. 1260
- (55) Pelucchi, M.; Cavallotti, C.; Cuoci, A.; Faravelli, T.; Frassoldati, 1261 A.; Ranzi, E. Detailed kinetics of substituted phenolic species in 1262 pyrolysis bio-oils. *React. Chem. Eng.* **2019**, *4* (3), 490–506. 1263
- (56) Wegeberg, C.; de Aguirre, A.; Maseras, F.; McKenzie, C. J. 1264 Photosynthesis of a Dihydroimidazopyridine Chelate Shines Light on 1265 the Reactions of a Photoactivated Iron(III) Complex with O₂. *Inorg.* 1266 *Chem.* **2020**, *59* (22), 16281–16290. 1267
- (57) Cong, J.; Kinschel, D.; Daniel, Q.; Safdari, M.; Gabrielsson, E.; 1268 Chen, H.; Svensson, P. H.; Sun, L.; Kloo, L. Bis(1,1-bis(2- 1269 pyridyl)ethane)copper(i/ii) as an efficient redox couple for liquid 1270 dye-sensitized solar cells. *J. Mater. Chem. A* **2016**, *4* (38), 14550– 1271 14554. 1272